Chapter 1

Structure of Ceramics

Atomic-level structure is a foundation for understanding the physical properties of materials. In this chapter we will discuss the idealized structure of crystalline and glassy ceramics, as the first level in a hierarchy of structures to be explored in subsequent chapters. The structure of perfect crystals is the basis for understanding defects in crystals and their many related physical properties, as discussed in Chapter 2. In Chapter 3, crystalline and defect structures are then used as the foundation for understanding mass and electrical transport in ceramics. Phase equilibria and microstructure-property relationships in single and polyphase ceramics, treated in Chapters 4 and 5, respectively, also cannot be meaningfully discussed without an understanding of the atomic-level structure of the phases involved.

Our principal objective in the following discussion will be to develop a systematic understanding of why particular crystal structures form, and how they may be predicted. Well-known ionic structures and their important derivatives are described, with an emphasis on viewing even complex structures from the basis of a few simple structure types. A second objective is to illustrate important relationships between the atomic arrangements of crystalline and glassy structures and the physical properties of ceramics, using examples with particular technological relevance.

Assumed Knowledge

As background, we will assume familiarity with general chemistry principles including the periodic table of the elements, the Bohr model of the atom, and the fundamentals of interatomic bonding. In the great majority of ceramic materials, it is ionic and covalent bonding that is of interest; ceramics with predominantly hydrogen bonding or metallic character exist but are relatively uncommon. With respect to the following discussion of crystal structures, a feature of particular importance is the *nondirectional* nature of the ionic bond compared to the *directional* nature of the covalent bond. This simply means that in the case of the ionic bond, electrostatic attraction is equally favorable in all directions and does not by itself promote a certain local bonding geometry. In contrast, the allowed geometries of the covalent bond are very much constrained by the electron orbital configuration. For example, the most commonly encountered type of covalent bonding in ceramic materials occurs where atoms have sp^3 hybridized orbitals, which may be visualized as extending in four lobes toward the vertices of a tetrahedron, with a symmetric interbond angle of 109.5°. This causes many covalently bonded ceramics to adopt a tetrahedral local coordination.

We will assume an elementary understanding of crystallography and of the system of Miller indices.[1] If not familiar, this information is available in a number of texts to which the reader may wish to refer, some listed at the end of the chapter. We will not emphasize the formal, crystallographic description of structures. A complete and quantitative description of crystals requires an identification of the periodicity (unit cell) of the structure, the three-dimensional symmetry, and the detailed positions of all atoms. There exists a widely accepted convention for describing these essential characteristics of crystals, embodied in an important reference known as the *International Tables for Crystallography*. The possible atomic arrangements of crystals are quantitatively described therein. However, while an understanding of this system is important background for the practicing materials scientist and engineer, it is a language that may not be familiar to many readers. In the interest of simplicity, we will only refer to it in passing. Sources for additional reading on the subject are given at the end of this chapter.

The theory of crystallography is extremely powerful in another respect; it permits the prediction of anisotropy in physical properties from crystal symmetry. We will discuss a number of properties that are related to crystal symmetry. Here also, a detailed discussion is not possible without a more extensive background in crystallography. The reader is referred in particular to the text by J. F. Nye, *Physical Properties of Crystals* (Clarendon Press, Oxford, 1957), for further reading on this topic.

[1] Whereby single crystallographic directions are referred to by the notation [hkl] and a family of directions by <hkl>, and a single crystallographic plane by (hkl) and a family of planes by {hkl}.

1.1 CLOSE-PACKED LATTICES

A majority of ceramic compounds crystallize in structures based on close packing of at least one of the atomic constituents. From the two simple close-packed lattice face-centered cubic (FCC) and hexagonal close packed (HCP)—most ionic crystals can be derived by the substitution of atoms into available *interstices*, the geometrically regular voids between atoms. It is generally the larger of the ions (usually the anion) that forms the close-packed structure, with the smaller ion or ions occupying the interstices. In the following discussion, we will often take the anion to be oxygen since so many important ceramics are oxides, but this anion may just as easily be, for example, a halogen ion (F, Cl, Br, I), nitrogen, or sulfur. In the case of high atomic number cations, for example zirconium and uranium, the cations may be larger than oxygen and the structure better viewed as a close-packed arrangement of cations, with oxygen inserted in the interstices. This is the basis of the fluorite structure, which we will use extensively as an example in this text. And, in some structures such as perovskite, the cations and anions are close in size and together form a close-packed lattice that is a convenient basis for viewing the crystal structure.

FCC and HCP Lattices

We begin by examining the characteristics of the FCC and HCP close-packed lattices, both of which consist of a sequential stacking of planar layers of close-packed atoms. These structures may be quite familiar; we will especially emphasize the location and number density of interstitial sites available to cations. Figure 1.1 shows one of the close-packed planes used to form an FCC or HCP lattice. Let's assume this to be an oxygen plane in a metal oxide crystal. Within the layer, each oxygen has six *nearest-neighbor* oxygen ions. Notice that in this hard-sphere representation, the oxygens are not in contact; this illustrates the situation in a real crystal where the anions are slightly separated from each other by the intervening cations. Thus the crystallographic unit cell size is determined by the size of the cation as well as the anion. We will arbitrarily call this an "A" layer, defining all positions that are directly above the centers of the oxygen atoms as "A" positions, whether they are occupied or not.

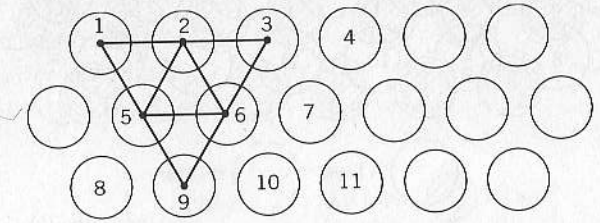

Fig. 1.1 Hexagonal close-packed layer of atoms.

We arrive at the FCC and HCP lattices by stacking like layers on top of this first layer, in the most densely packed arrangement possible. This is achieved by nesting the oxygen atoms of the next layer in the depressions between three oxygen atoms in the A layer, Fig. 1.1. The spacing of atoms in the next close-packed layer "B" requires that every other triangular array of atoms in layer A be occupied. Such positions are defined by atoms 1, 2, 5 and 2, 3, 6 in Fig. 1.1. Figure 1.2 shows how this B layer of close-packed oxygen atoms is positioned with respect to the A layer. The two are identical except for a lateral translation; the B-layer atoms are denoted in Fig. 1.2 by lowercase letters and do not lie directly above any of the A-layer atoms.

Continued stacking of close-packed layers on top of the B-layer generates the FCC and HCP lattices. The FCC lattice is formed when a third layer is stacked with its atoms nested in the triangular arrays of atoms in the B layer that have their apex downward in the orientation of Fig. 1.3. It turns out that these positions do not lie directly over atoms in either the A or B layer, and so we denote it as a "C" layer (shown shaded). The FCC lattice repeats when a fourth layer is added over C with its atoms directly above those in A. (Here again the new layer occupies triangles in the C layer that have their apex pointing downward on the page.) The FCC stacking sequence (ABCA) is then repeated indefinitely to form the lattice: ABCABCABC.... Even though this lattice is made by a stacking sequence of hexagonal planar layers, in three dimensions the unit cell is cubic. A perspective showing the cubic FCC unit cell appears in Fig. 1.4, where the {111} planes of atoms are the original A, B, C, and A layers of close-packed oxygen ions. If the unit cell in Fig. 1.4 is oriented so that the body diagonal (a ⟨111⟩ direction) is vertical, we then obtain the side-view perspective in Fig. 1.6 showing clearly the ABCA.... stacking sequence.

The HCP lattice is formed by stacking another A layer directly above the A–B layer sequence shown in Fig. 1.2. Figure 1.5 shows this arrangement, where the second A layer is now directly above the initial one. Notice that this results from the second A layer being nested in triangular arrays of atoms in the B layer which

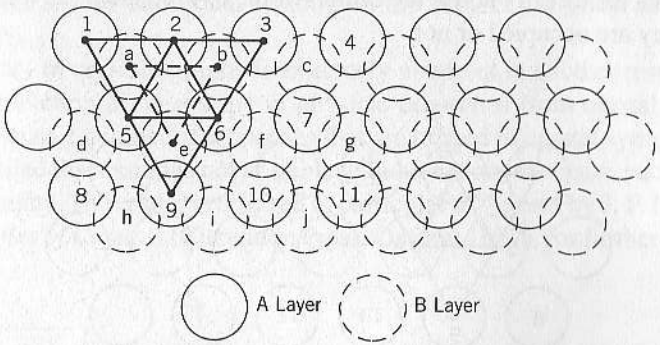

Fig. 1.2 Close-packing of two atomic layers.

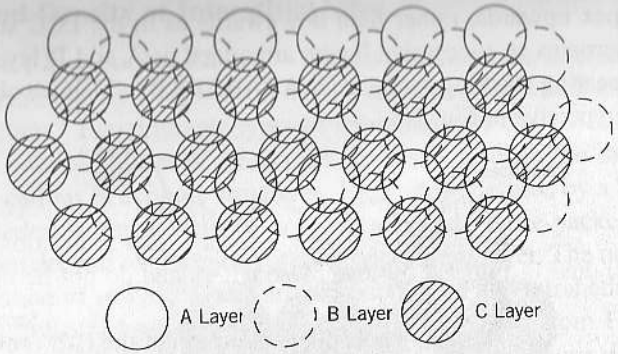

Fig. 1.3 A-B-C close-packing of the FCC structure.

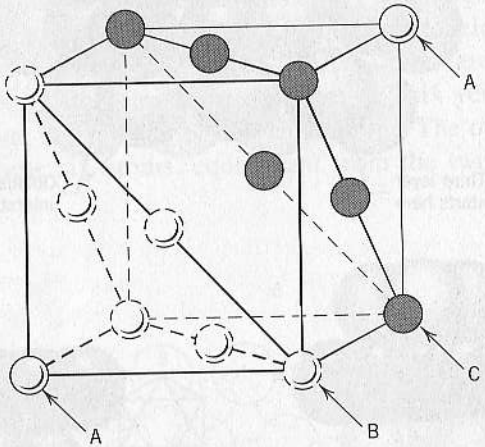

Fig. 1.4 A-B-C-A stacking of close-packed layers in the FCC structure. Each plane is normal to the body diagonal (a <111> type direction).

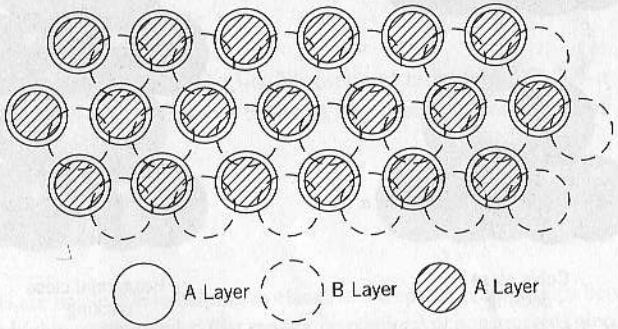

Fig. 1.5 A-B-A close-packing of the HCP structure.

have their apex upwards, rather than downwards as in the FCC structure. This sequence alternates as successive layers are added as A and B layers. The final infinitely-repeating stacking sequence is ABABABAB, which we observe from a side-view perspective in Fig. 1.6.

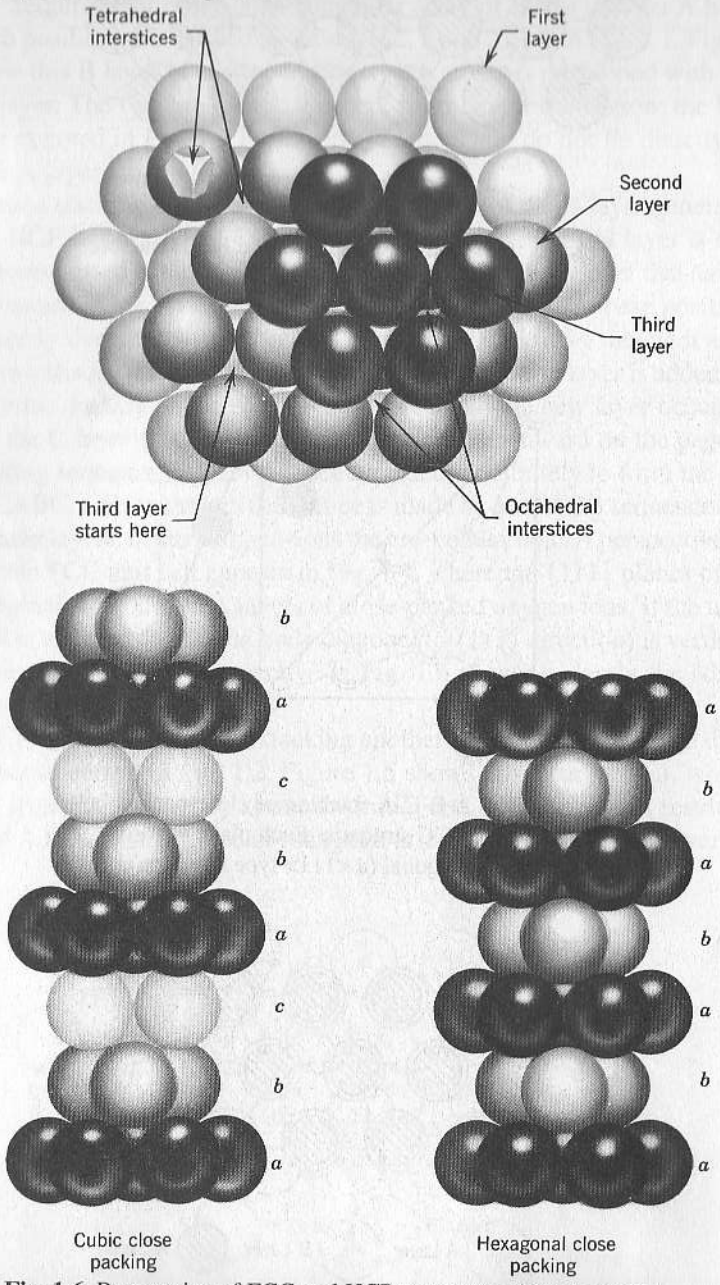

Fig. 1.6 Perspective of FCC and HCP structures viewed parallel to close-packed layers.

Location and Density of Interstitial Sites

Sites Between Close-Packed Layers. We now examine the interstices, defined as the polyhedral cavities formed between packed atoms, which exist in close-packed structures.[2] Two principle types of interstitial sites, *tetrahedral* and *octahedral*, exist between layers of close-packed ions. These are the most common locations for cations in ceramic structures. Each site is defined by a local *coordination polyhedron* formed between any two adjoining close-packed layers and which does not depend on the configuration of the third layer. The nearest-neighbor configuration of oxygen atoms around octahedral and tetrahedral cations is thus independent of whether the basic structure is derived from FCC or HCP. From this fact we deduce directly that *FCC and HCP lattices have the same number density of octahedral and tetrahedral sites.*

The location of interstitial sites between an A and B layer are illustrated in Fig. 1.7, where the atoms are labeled the same way as in Figs. 1.1 and 1.2. A single octahedral site is defined by the six oxygen atoms labeled 3, 6, 7, and b, c, f; i.e., three of these atoms are in the A layer and three are in the B layer. (Recall that a regular octahedron has eight sides and six vertices; therefore these six atoms define the vertices of the octahedron.) The octahedral site is centered between these six atoms, equidistant from the two oxygen close-

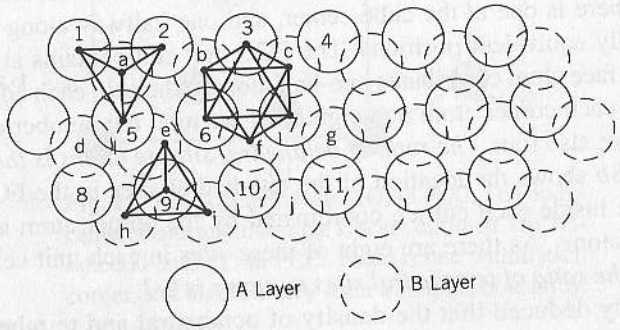

Fig. 1.7 Octahedral (3-6-7-b-c-f) and tetrahedral (1-2-5-a and e-h-i-9) interstices between two close-packed layers of atoms.

[2]Physical models are invaluable in helping to visualize the spatial relationships between atoms and interstitials. It is highly recommended that models be obtained or constructed (glued-together ping-pong balls or styrofoam balls are effective) for better visualization.

packed layers. This site is neither directly above nor directly below the atoms in the oxygen layers (A and B). It is co-linear with third layer C atom if the three-dimensional arrangement is FCC). Upon identifying the other octahedral sites between the A and B atomic layers, we find that the octahedral sites together form a hexagonal array, centered halfway between the adjacent close-packed layers and with the same periodicity as the close-packed atoms.

Turning now to the tetrahedral sites, we find that there are two different types defined by any two adjacent close-packed oxygen layers. One group of tetrahedra are defined by having three A-layer atoms and one B-layer atom (see the atoms labeled 1, 2, 5, and a). These tetrahedra can be visualized as having an apex pointing out of the plane of the paper. The other group of tetrahedra are defined by three B-layer atoms and one A-layer atom (see the atoms labeled e, h, i, and 9), and have an apex pointing into the plane of the plane of the paper. Upon identifying all sites of each type, it can be seen that a hexagonal array of each exists as well.

Note that the geometric centers of the tetrahedral sites, unlike those of the octahedral sites, are not exactly halfway between the adjacent oxygen planes but are slightly closer to the plane that forms the base of the tetrahedron. For all tetrahedral sites the center of the tetrahedron is either directly above or directly below an atom in one of the adjacent oxygen layers.

Three-Dimensional Arrangements of Interstitial Sites. Let's now examine the position of these sites with respect to the conventional depiction of the FCC and HCP unit cells. Figure 1.8*a* shows the location of the octahedral sites in the FCC structure: There is one at the cube center, and one halfway along each edge at symmetrically equivalent positions. The FCC unit cell contains at total of four atoms (each face atom contributes one-half atom to the cell, each edge atom one-quarter, and each corner atom one-eighth). If we total the number of octahedral sites, there are also four. *The ratio of octahedral sites to atoms is therefore 1:1.*

Figure 1.8*b* shows the location of the tetrahedral sites in the FCC structure. There is one inside each corner, coordinated by the corner atom and the three closest face atoms. As there are eight of these sites in each unit cell containing four atoms, *the ratio of tetrahedral sites to atoms is 2:1.*

We already deduced that the density of octahedral and tetrahedral sites is the same in FCC and HCP. In Fig. 1.9, the locations of each type of site in the HCP unit cell are shown. It is somewhat more difficult to visualize than in the FCC structure; we find two tetrahedral sites contained entirely within the cell above and below the body atom, and two on each vertical edge of the cell. The total number is therefore four tetrahedral sites per unit cell. Since this cell contains just two atoms, the ratio of tetrahedral sites to atoms is 2:1. There are two octahedral sites per unit cell, situated within the unit cell as shown in Fig. 1.9, for the expected site to atom ratio of 1:1. Notice that the octahedral sites form continuous rows oriented normal to the close-packed atom planes of the HCP structure.

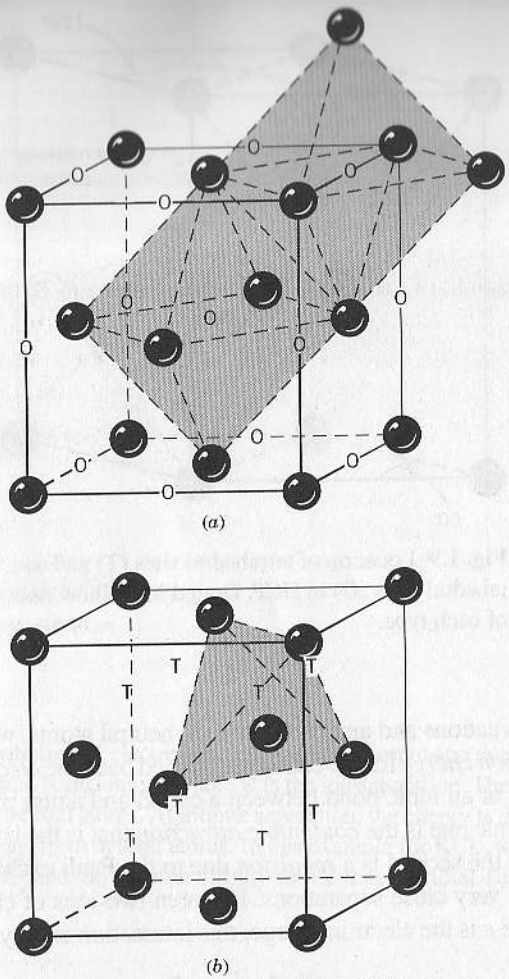

Fig. 1.8 (*a*) Octahedral sites (O) in FCC. The body-centered site and one edge site are outlined. (*b*) Tetrahedral sites (T) in FCC. There is one within each corner, and together they form a simple cubic array.

1.2 STABILITY OF IONIC CRYSTAL STRUCTURES

The Madelung Constant

With this understanding of the atom and interstitial positions in the FCC and HCP structures, we can now develop a geometric approach to ceramic crystal structures through the systematic filling of interstices. First, however, let us consider the question of energetic stability. That is, why is an ionic crystal preferred over the same number of isolated molecules? The *Madelung constant* is a precise definition of the energy of a particular crystal structure relative to the same number of isolated molecules.

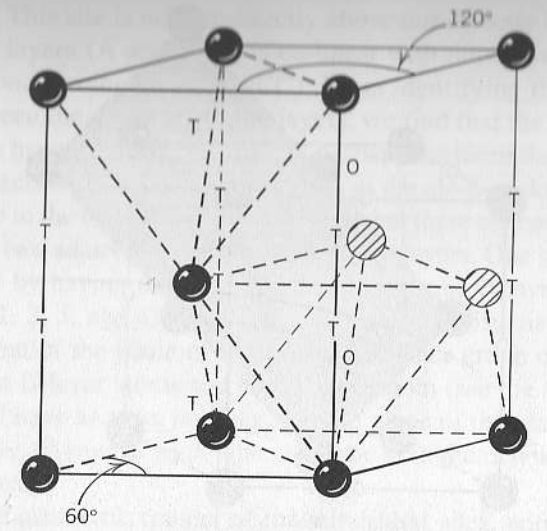

Fig. 1.9 Location of tetrahedral sites (T) and octahedral sites (O) in HCP. Dotted lines show one of each type.

Beginning with cations and anions rather than neutral atoms, we have already expended the *ionization energy* for the cation and gained back the *electron affinity* for the anion. The energy of an ionic bond between a cation and anion pair can then be described by two terms: one is the *coulombic attraction* that is the basis for the bond in the first place, and the second is a *repulsion* due to the Pauli exclusion principle that becomes strong at very close separations. Between two ions of charge $Z_i e$ and $Z_2 e$, respectively, where e is the electron charge, this interaction energy has the form:

$$E = \frac{Z_i Z_j e^2}{4\pi\varepsilon_0 R_{ij}} + \frac{B_{ij}}{R_{ij}^{\,n}} \tag{1.1}$$

where ε_o is the permittivity of free space, B_{ij} is an empirical constant, R_{ij} is the interatomic separation, and the exponent n has a value of ~10. The contributions of these two terms to the ionic bond are shown in Fig. 1.10 for the example of KCl. For attractive bonds there exists an equilibrium separation R_0 given by the sum of the cation and anion radii at which the total energy is a minimum, which we will denote as E_0.

Consider now a crystal composed of N such molecules. As separate pairs, the energy of the whole would be NE_0. In order for the crystal to form and be stable, its energy must be less than NE_0. The interaction energy of the crystal is obtained by summing the interaction of each of the $2N$ ions in the crystal, using Eq. 1.1, with every other ion in the crystal (and dividing by two to avoid counting interactions between any ions i and j twice). This summation includes interactions be-

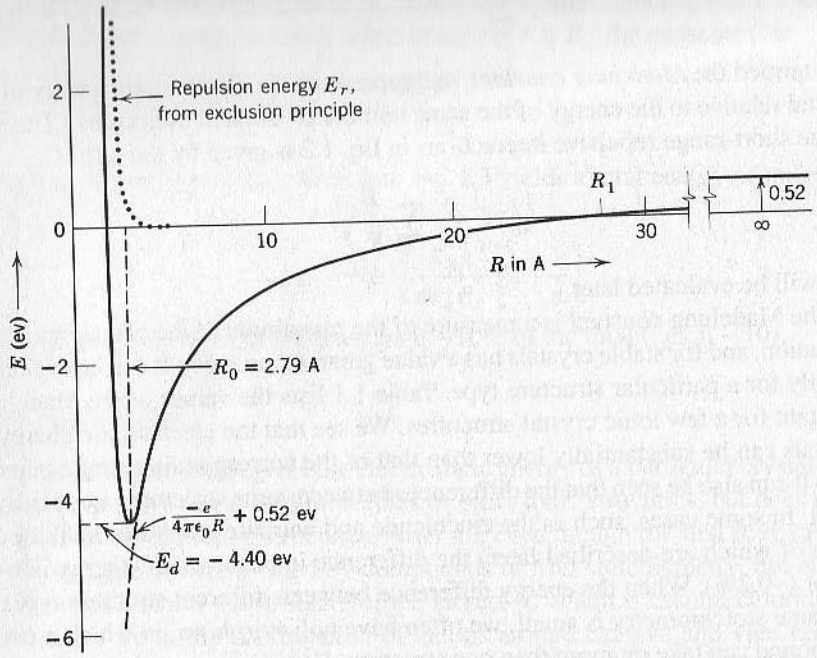

Fig. 1.10 Contribution of electrostatic attraction and repulsion due to Pauli exclusion to the ionic bond energy, where R is the ion separation. The energy zero is referenced to neutral atoms. At infinite separation, the energy is that for forming individual ions from neutral atoms. In this example for KCL, the ionization energy to form K^+ and the electron affinity for Cl^- together total +0.52 eV.

tween ions of like charge for which the energy is repulsive as well as those of opposite charge for which it is attractive, and for a crystal of N molecules is:

$$E_C = N\sum_j \left[\frac{Z_i Z_j e^2}{4\pi\varepsilon_0 R_{ij}} + \frac{B_{ij}}{R_{ij}^{\,n}} \right] \tag{1.2}$$

Eq. 1.2 can be rewritten in a form that allows the summation terms to be separated. For a compound of formula "MX" in which the cation valence is Z_c and the anion valence is Z_a, upon writing the separation between ions as $R_{ij} = x_{ij} R_0$, where R_0 is the minimum possible separation (the sum of the ionic radii, $R_o = R_A + R_c$), we have

$$E_C = N\left[\alpha \frac{Z_C Z_A e^2}{4\pi\varepsilon_0 R_0} + C \right] \tag{1.3}$$

In this relation α is the summation of the electrostatic interactions, given by:

$$\alpha = -\sum_i \frac{(Z_i/|Z_i|)(Z_j/|Z_j|)}{X_{ij}} \tag{1.4}$$

α is termed the *Madelung constant*, and represents the electrostatic energy of the crystal relative to the energy of the same number of isolated molecules.[3] The sum of the short-range repulsive interactions in Eq. 1.2 is given by the term C:

$$C = -\sum_i \frac{B_{ij}}{X_{ij}^{\,n}} \tag{1.5}$$

and will be evaluated later.

The Madelung constant is a measure of the magnitude of the electrostatic stabilization, and for stable crystals has a value greater than unity. It can be evaluated exactly for a particular structure type. Table 1.1 lists the values of the Madelung constant for a few ionic crystal structures. We see that the electrostatic energy of crystals can be substantially lower than that of the corresponding single pairs of ions. It can also be seen that the differences between some structures are relatively small. In some cases, such as the zincblende and wurtzite structures in Table 1.1 (both of which are described later) the difference in electrostatic energy is truly minor (~0.2%). When the energy difference between different structure types of the same stoichiometry is small, we often have *polymorphism*, in which a single compound can take on more than one structure.

For ionic crystals the majority of the interaction energy lies in the electrostatic term, with the short-range repulsion accounting for only about 10% of the interaction. We show this to be the case by first noting that the energy of interaction is a minimum at an ion separation of R_0. Then, upon differentiating Eq. 1.2 with respect to R and setting the result equal to zero at $R = R_0$, the constant C is

$$C = -\alpha \frac{Z_C Z_A e^2}{4\pi\varepsilon_0} R_o^{\,n-1} \tag{1.6}$$

Substituting this expression back into Eq. 1.3 yields a total energy of interaction of

$$E_C = N\alpha \frac{Z_C Z_A e^2}{4\pi\varepsilon_0 R_0}\left[1 - \frac{1}{n}\right] \tag{1.7}$$

where the second term in the brackets is ~10% of the total (i.e., n ~ 10).

Table 1.1 Madelung Constants for Some Common Ionic Crystal Structures

Structure Type	α
Rocksalt	1.748
Cesium Chloride	1.763
Zincblende	1.638
Wurtzite	1.641
Fluorite	2.519
Corundum	4.040

[3]This statement is strictly true only for compunds "MO" of 1:1 stoichiometry, such as NaCl, MgO, ZnO. For other stoichiometries, such as M_2O, MO_2, and M_2O_3, the electrostatic energy of an isolated molecule is no longer given exactly by the term $Z_cZ_ae^2/4\pi\varepsilon_0R_0$. We may still use this term as an energy reference and use Eq. 1.3 to define the Madelung constant, α, as the energy of the crystal relative to this value. However, α is no longer given by the summation in Eq. 1.4. Some other conventions are also used to define the Madelung constant, as discussed in greater detail in D. Quane, *J. Chem. Education*, **47**[5], 396 (1970) and the original references contained therein.

Pauling's Rules

The Madelung constant gives the electrostatic energy of a particular crystal structure type relative to isolated molecules or other ionic structures, but does not by itself allow us to predict structures. After all, even though the first four structure types in Table 1.1 are formed by compounds of MO stoichiometry, not all such compounds form in the structure of the largest α, which is cesium chloride. The differences lie in the coordination of anions around cations, and vice versa, in these respective structures. In any structure with a large fraction of ionic bonding character, minimum electrostatic energy is achieved when cation–anion attractions are maximized and like-ion electrostatic repulsion is minimized. That is, cations prefer to be surrounded by the maximum number of anions as *first nearest neighbors*, and vice versa. At the same time, however, cations prefer to maintain maximum separation from the other cations that are their *second nearest neighbors*. Another way of saying this is that ions of like charge prefer to be electrostatically "shielded" from one another as much as possible by ions of the opposite charge. Often, the larger of the ions will form an FCC or HCP array, the interstices of which are occupied by the oppositely charged ion in an orderly way. However, any such arrangement must conform to the need for local charge neutrality, which when extended over the entire crystal maintains the *stoichiometry* or cation/anion ratio of the compound.

Pauling's rules are a set of five general statements, given as follows in approximate order of decreasing influence, which allow us to understand how known ionic structures satisfy the preceding requirements. Conversely, we may use them to predict the structure in which a compound is likely to crystallize. Pauling's rules are based on the geometric stability of packing for ions of different sizes, combined with simple electrostatic stability arguments. These geometric arguments treat ions as hard spheres, which is clearly an oversimplification. However, while ionic radii (as defined by interatomic spacings) do vary from compound to compound, they tend to vary most strongly with the valence state of the ion and the number of nearest-neighbor ions of the opposite charge. Thus for present pur-

poses we will consider an ionic radius to be constant for a particular valence state and a nearest-neighbor coordination number. This is a useful approximation supported by empirical observations of the interatomic spacings (determined by the sum of cation and anion radii) in a wide variety of oxides and halides. In general, ion size increases as valence decreases (as electrons are added) and also increases as the number of nearest neighbors increases. These trends can be seen in Table 1.2, which lists ionic radii from the 1976 tabulation of R. D. Shannon. Data for octahedral (CN = 6) and tetrahedral (C N = 4) coordination, and some radii for CN = 8 and 12 are included.

Rule 1 Pauling's first rule states that each cation will be coordinated by a polyhedron of anions, the number of ions in which is determined by the relative sizes of the cation and anion. When anions form a regular polyhedron, there is a single characteristic size for the interstice if the anions (assumed to be spherical) are in contact. For instance, the largest sphere that can fit in the tetrahedral and octahedral interstices of the FCC and HCP arrays when all atoms are touching can be calculated to be 0.225 and 0.414 times the radius of the close-packed atom. The filling of an interstice by a cation smaller than this characteristic size (and which therefore can rattle about) tends to be unstable. A stable configuration is obtained when the cation is as large or slightly larger than this characteristic dimension, as depicted in Fig. 1.11. (Recall that in Figs. 1.1 and 1.2 we showed the close-packed anion arrays as slightly separated to account for the intervening cations in the interstices.) Beyond a certain cation size, however, a larger polyhedron becomes necessary.

We can therefore determine from the cation/anion *radius ratio*, r_C/r_A, the largest polyhedron for which the cation can completely fill the interstice. This is then the local structural unit most likely to form. These polyhedra and the corresponding limiting radius ratios are shown in Fig. 1.12. When the radius ratio is less than this geometrically determined critical value, the next lower coordination becomes preferred. (Remember, however, that a different effective radius applies when we change coordination number.) Although the above is concerned with cations that are smaller than the anion, some important compunds exist for which the reverse is true. In those instances, we can apply the same principle using a cation coordi-

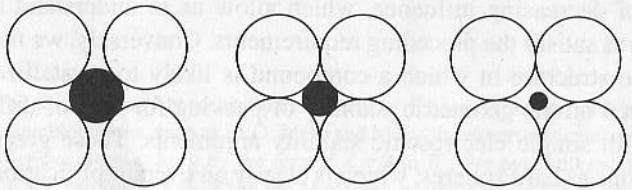

Fig. 1.11 Stable and unstable coordination configurations.

Table 1.2 Ionic Crystal Radii (nm)

Coordination Number = 6														
Ag^{1+}	Al^{3+}	As^{5+}	Au^{1+}	B^{3+}	Ba^{2+}	Be^{2+}	Bi^{3+}	Bi^{5+}	Br^{1-}	C^{4+}	Ca^{2+}	Cd^{2+}		
0.115	0.054	0.046	0.137	0.027	0.135	0.045	0.103	0.076	0.196	0.016	0.100	0.095		
Ce^{4+}	Cl^{1-}	Co^{2+}	Co^{3+}	Cr^{2+}	Cr^{3+}	Cr^{4+}	Cs^{1+}	Cu^{1+}	Cu^{2+}	Cu^{3+}	Dy^{3+}	Er^{3+}		
0.087	0.181	0.075	0.055	0.080	0.062	0.055	0.167	0.077	0.073	0.054	0.091	0.089		
Eu^{3+}	F^{1-}	Fe^{2+}	Fe^{3+}	Ga^{3+}	Gd^{3+}	Ge^{4+}	Hf^{4+}	Hg^{2+}	Ho^{3+}	I^{1-}	In^{3+}	K^{1+}		
0.095	0.133	0.078	0.065	0.062	0.094	0.053	0.071	0.102	0.090	0.220	0.080	0.138		
La^{3+}	Li^{1+}	Mg^{2+}	Mn^{2+}	Mn^{4+}	Mo^{3+}	Mo^{4+}	Mo^{6+}	N^{5+}	Na^{1+}	Nb^{5+}	Nd^{3+}	Ni^{2+}		
0.103	0.076	0.072	0.083	0.053	0.069	0.065	0.059	0.013	0.102	0.064	0.098	0.069		
Ni^{3+}	O^{2-}	OH^{-}	P^{5+}	Pb^{2+}	Pb^{4+}	Rb^{1+}	Ru^{4+}	S^{2-}	S^{6+}	Sb^{3+}	Sb^{5+}	Sc^{3+}		
0.056	0.140	0.137	0.038	0.119	0.078	0.152	0.062	0.184	0.029	0.076	0.060	0.075		
Se^{2-}	Se^{6+}	Si^{4+}	Sm^{3+}	Sn^{4+}	Sr^{2+}	Ta^{5+}	Te^{2-}	Te^{6+}	Th^{4+}	Ti^{2+}	Ti^{3+}	Ti^{4+}		
0.198	0.042	0.040	0.096	0.069	0.118	0.064	0.221	0.056	0.094	0.086	0.067	0.061		
Tl^{1+}	Tl^{3+}	U^{4+}	U^{5+}	U^{6+}	V^{2+}	V^{5+}	W^{4+}	W^{6+}	Y^{3+}	Yb^{3+}	Zn^{2+}	Zr^{4+}		
0.150	0.089	0.089	0.076	0.073	0.079	0.054	0.066	0.060	0.090	0.087	0.074	0.072		

Continued

Coordination Number	Disposition of Ions about Central Ion	Range of – Cation Radius Ratio Anion Radius
8	Corners of cube	≥ 0.732
6	Corners of octahedron	≥ 0.414
4	Corners of tetrahedron	≥ 0.225
3	Corners of triangle	≥ 0.155
2	Linear	≥ 0

Fig. 1.12 Critical radius ratios for various coordination numbers. The most stable structure is usually the one with the maximum coordination number allowed by the radius ratio.

nation polyhedron as a structural unit, and use the anion/cation radius ratio to determine the likely coordination number for cations around anions. The fluorite structure discussed later is an example of of such structures.

Exceptions to the exact statement of Pauling's first rule are not difficult to find and occur because ions are not really hard spheres as assumed, but are somewhat deformable. Local electrical neutrality requirements as discussed for the follow-

Coordination Number = 4										
Ag^{1+}	Al^{3+}	As^{5+}	B^{3+}	Be^{2+}	C^{4+}	Cd^{2+}	Co^{2+}	Cr^{4+}	Cu^{1+}	Cu^{2+}	F^{1-}	Fe^{2+}
0.100	0.039	0.034	0.011	0.027	0.015	0.078	0.058	0.041	0.060	0.057	0.131	0.063
Fe^{3+}	Ga^{3+}	Ge^{4+}	Hg^{2+}	In^{3+}	Li^{1+}	Mg^{2+}	Mn^{2+}	Mn^{4+}	Na^{1+}	Nb^{5+}	Ni^{2+}	O^{2-}
0.049	0.047	0.039	0.096	0.062	0.059	0.057	0.066	0.039	0.099	0.048	0.055	0.138
OH^-	P^{5+}	Pb^{2+}	S^{6+}	Se^{6+}	Sn^{4+}	Si^{4+}	Ti^{4+}	V^{5+}	W^{6+}	Zn^{2+}		
0.135	0.017	0.098	0.012	0.028	0.055	0.026	0.042	0.036	0.042	0.060		

Coordination Number = 8							
Bi^{3+}	Ce^{4+}	Ca^{2+}	Ba^{2+}	Dy^{3+}	Gd^{3+}	Hf^{4+}	
0.117	0.097	0.112	0.142	0.103	0.105	0.083	
Ho^{3+}	In^{3+}	Na^{1+}	Nd^{3+}	O^{2-}	Pb^{2+}	Rb^{1+}	
0.102	0.092	0.118	0.111	0.142	0.129	0.161	
Sr^{2+}	Th^{4+}	U^{4+}	Y^{3+}	Zr^{4+}			
0.126	0.105	0.100	0.102	0.084			

Coordination Number = 12				
Ba^{2+}	Ca^{2+}	La^{3+}	Pb^{2+}	
0.161	0.134	0.136	0.149	
Sr^{2+}				
0.144				

Source: R. D. Shannon, *Acta Crystallographica*, A32, 751 (1976).

ing rule can result in a different coordination number than the first rule predicts, particularly for high atomic number elements. Covalent and metallic bonding character also tend to shorten interatomic distances compared to highly ionic bonds.

Rule 2 This rule ensures that the basic coordination polyhedra are arranged in three dimensions in a way that preserves local charge neutrality. A cation–anion "bond strength" is defined as *the valence of the ion divided by its coordination number*. Taking the compound MgO as an example, octahedrally coordinated Mg^{2+} will have a bond strength of 2/6. This is qualitatively a measure of the relative fraction of the 2+ charge that is being allocated to or shared with each of the coordinating anions. Next, the oxygen anion must be coordinated by sufficient cations to satisfy its 2– valence. This is achieved when *the sum of the bond strengths reaching the ion equals its valence*. This means that in MgO each oxygen atom must be coordinated by six Mg^{2+} ions: $6 \times (2/6) = 2$. In multicomponent compounds an anion may be coordinated by more than one type of cation, in which case each cation may have a different bond strength. Still, the sum of all bond strengths to the anion must equal its valence. This calculation of the contribution of bond strength to local charge neutrality can be performed around either the cation or the anion, and must be satisfied for both. In applying the second rule it thus becomes important to understand the coordination of *cations around anions* as well as those of *anions around cations*.

Rule 3 Coordination polyhedra prefer linkages where they share corners rather than edges, and edges rather than faces. This rule is simply based on the fact that cations prefer to maximize their distance from other cations in order to minimize electrostatic repulsion. (With model polyhedra, one can visualize the decreasing distance between cations upon proceeding from corner-sharing to edge-sharing to face-sharing.) Notice that this preference must be balanced by the fact that corner sharing does not always permit local charge neutrality since it restricts the number of cations that can coordinate an anion (see the second rule).

Rule 4 This rule states that rule 3 becomes more important when the coordination number is small or the cation valence high. A prime example is SiO_2, in which SiO_4^{4-} tetrahedra are linked at corners. This also is based on electrostatics; the repulsive energy between a pair of cations is proportional to the charge squared and inversely proportional to their separation.

Rule 5 Simple structures are usually preferred over more complicated arrangements. For example, when several cations of similar size and identical valence are incorporated into a lattice, they frequently occupy the same type of site but are distributed at random, forming a solid solution or "alloy." As the cations become increasingly dissimilar (and as temperature is lowered), a tendency to form an ordered arrangement or "superlattice" may occur. Finally, when the cations are sufficiently different, they may each take on entirely different coordinations increasing the complexity of the structure.

In summary, then, how can we apply Pauling's rules to deduce the unknown structure of an ionic compound? If the cation is smaller than the anion, as is often the case, we can deduce that FCC or HCP close-packing of the anions will occur. The cation/anion radius ratio helps us to decide which interstitial sites will be occupied; and by far the most common are octahedral and tetrahedral sites. Then, keeping in mind the ratio of interstitial sites to atoms in the FCC and HCP structures, we examine the stoichiometry of the compound. For example, a binary metal oxide MO has a 1:1 cation to anion ratio, so if octahedral coordination (CN = 6) is preferable, we can deduce that all of the octahedral sites will be filled since the ratio of octahedral sites to atoms is also 1:1. If tetrahedral coordination (CN = 4) is preferred, then only one-half of the tetrahedral sites need be filled since the ratio of tetrahedral sites to atoms is 2:1. These sites will tend to be filled in a way that maximizes the cation separation, according to Pauling's third and fourth rules. What follows is a straightforward analysis that helps us understand the more common ceramic structures.

1.3 CERAMIC CRYSTAL STRUCTURES

The majority of ceramic crystal structures are based on either FCC or HCP close-packing of one type of ion, with the other ion(s) occupying a specific set of interstitial sites. We will discuss some of the most important structures, beginning with those based on FCC anion close-packing with the cations occupying octahedral sites. Then, structures that are based on occupation of tetrahedral sites will be considered. Finally, we will discuss some structures of mixed occupancy. Table 1.3 lists a number of representative compounds for each crystal structure type.

For example, the *rocksalt* structure, which is the simplest and perhaps most familiar of the FCC-based structures, has all of the octahedral sites filled with cations. A corresponding FCC structure with all tetrahedral sites occupied is *antifluorite*. On the other hand, the *zincblende* structure has only one-half of the tetrahedral sites filled. It is closely related to the diamond cubic structure, which is that of the diamond phase of carbon as well as the elemental semiconductors silicon and germanium. The *perovskite* structure, which is quite important for understanding ferroelectric materials and ceramic superconductors, is loosely based on an FCC-based structure with octahedral site filling, but here the FCC array includes both anions and cations.

Perhaps the most important example of an HCP-based oxide with octahedral site filling is *corundum*, the structure of the widely used ceramic, aluminum oxide (Al_2O_3). It is based on the HCP stacking of oxygen with $^2/_3$ of the octahedral sites filled. We will examine this and some closely related derivative structures: $LiNbO_3$ and $FeTiO_3$. (Derivative structures are more complex structures that can be derived, and are most easily understood, using a simpler structure.) A tetrahedrally

Table 1.3 Some Ceramic Crystal Structures

Structure	Stoichiometry	Anion Packing	Coordination Number around M and X	Examples	Derivative Structures
Rocksalt	MX	FCC	6, 6	NaCl, KCl, LiF, KBr MgO, CaO, SrO, BaO NiO, CoO, MnO, FeO, TiN, ZrN	
Zincblende	MX	FCC	4, 4	ZnS, BeO, SiC (3C), BN,GaAs, CdS, InSb	Diamond cubic (Si, Ge, C)
Wurtzite	MX	HCP	4, 4	ZnO, ZnS, AlN, SiC (2H)	
Nickel arsenide	MX	HCP	6, 6	NiAs, FeS, FeSe, CoSe	
Anti-fluorite	M_2X	FCC	4, 8	Li_2O, Na_2O, K_2O Rb_2O	
Fluorite	MX_2	Primitive cubic	8, 4	CaF_2, ZrO_2, UO_2, ThO_2, CeO_2	Pyrochlore ($A_2B_2O_7$), e.g., $Pb_2Ru_2O_7$, $Gd_2Ti_2O_7$, $Gd_2Zr_2O_7$ Bixbyite (e.g. Y_2O_3)
Cesium Chloride	MX	Primitive cubic	8, 8	CsCl, CsBr, CsI	
Rutile	MX_2	Distorted HCP	6, 3	TiO_2, SnO_2, GeO_2 MnO_2, VO_2, NbO_2 RuO_2, PbO_2, PbO_2	Defective "Magneli phases" of formula Ti_nO_{2n-1}

Table 1.3 *continued*

Corundum	M_2X_3	HCP	6, 4	Al_2O_3, Cr_2O_3	Ilmenite ($FeTiO_3$) Lithium Niobate ($LiNbO_3$, $LiTaO_3$)
Perovskite	ABX_3	AO sublattice forms FCC	12, 6, 6	$CaTiO_3$, $SrTiO_3$ $BaTiO_3$, $PbTiO_3$ $LaGaO_3$, $LaAlO_3$ $BaZrO_3$, $PbZrO_3$ $Ba(Pb_{1-x}Bi_x)O_3$, $Ba_{1-x}K_xO_3$ $Pb(Zr, Ti)O_3$ $(Pb, La)(Zr, Ti)O_3$	Ordered solid solutions, e.g., $Pb(Mg_{1/3}Nb_{2/3})O_3$, $Pb(Sc_{1/2}Ta_{1/2})O_3$
Spinel	AB_2X_4	FCC	4, 6, 4	$MgAl_2O_4$, $FeAl_2O_4$ $ZnAl_2O_4$, $ZnFe_2O_4$ $MnFe_2O_4$, $LiTi_2O_4$	Many solid solutions are possible.
Inverse spinel	$B(AB)X_4$	FCC	4, 6, 4	Fe_3O_4, $CoFe_2O_4$ $NiFe_2O_4$, $MgFe_2O_4$	Many solid solutions.
"K_2NiF_4"	A_2BX_4	Alternating perovskite and rocksalt type layers	9, 6, 6	K_2NiF_4, La_2CuO_4 $La_{2-x}Sr_xCuO_4$, La_2NiO_4	"Ruddlesden-Popper" phases $AO{\cdot}nABO_3$, e.g., Sr_2TiO_4, $Sr_3Ti_2O_7$; high temperature oxide superconductors of formula $mAO{\cdot}nABO_3$ such as $Bi_2Sr_2CaCu_2O_8$, $Tl_2Ba_2Ca_2Cu_3O_{10}$.

Table 1.3 *continued*

"$YBa_2Cu_3O_7$"	$AB_2C_3X_7$	Perovskite-like with missing oxygens	8, 10, 5 or 4, 6	$YBa_2Cu_3O_7$, $MBa_2Cu_3O_7$, where M = Eu, Dy, Ho, Er, Yb	$Y_2Ba_4Cu_7O_x$, $Y_2Ba_4Cu_8O_x$
Silicates (quartz, tridymite crystobalite)	AX_2	Corner-shared SiO_4 tetrahedra	4, 2	SiO_2, GeO_2	β-eucryptite ($LiAlSiO_4$) is a quartz derivative; many other crystalline silicates of similar coordination; network glasses.
Silicon nitride	A_3X_4	Corner shared SiN_4 tetrahedra	4, 3	α- Si_3N_4, β-Si_3N_4	Silicon oxynitrides solid solutions (sialons) with valence-compensating cation and anion substitutions.

filled HCP structure of importance is *wurtzite*, in which one half of the tetrahedral sites are filled. (ZnO is one example.) A final HCP-based structure we will examine is *rutile*, the mineral name of the compound TiO_2, in which one-half of the octahedral sites are also filled, but in such a way that the resulting symmetry of the crystal is actually tetragonal.

The structures of ceramics with a large degree of covalent bonding are not determined by Pauling's rules, but by the directional bonding. These are discussed later. Coincidentally, however, some of the simpler ionic structures also satisfy this requirement. Two such structures are zincblende and wurtzite, in which all atoms have a tetrahedral nearest-neighbor coordination satisfying the tetrahedral sp^3 hybridized orbital orientation.

FCC-Based Structures

Rocksalt. This structure consists of an FCC anion lattice in which all octahedral sites are filled with cations. The radius ratio r_C/r_A should be between 0.414 and 0.732 according to Pauling's first rule, and since the ratio of octahedral sites to atoms in FCC is 1:1, compounds of this structure have an ideal stoichiometry of MX. (There are cases such as $Fe_{1-x}O$ where a deficiency exists on one sublattice, discussed later when we consider lattice defects.) Examples of ceramic materials that form this structure include NaCl, KCl, LiF, MgO, CaO, SrO, NiO, CoO, MnO, and PbO. For all of these, the anion is the larger and forms the FCC lattice. Figure 1.13*a* shows one unit cell of the rocksalt structure. The lattice constant of the cubic unit cell is "a" and each unit cell contains four formula units.

Let's examine the structure with respect to Pauling's second rule, for the cases of NaCl and MgO. For NaCl the bond strength contributed by a cation is 1/6. The coordination number of anions around cations is the same as that of cations around anions: six. Therefore the sum of bond strengths reaching a chlorine ion is the valence of the chlorine ion ($6 \times (1/6) = 1$) as predicted by the second rule. For MgO, the bond strength is 2/6 and the sum of bond strengths reaching the oxygen ion is $6 \times (2/6) = 2$, the valence of the oxygen ion. Upon examining the structure closely, we find that the octahedra share edges. If they were to share corners, we would have a coordination of two cations per anion and the second rule would not be satisfied.

In order to help visualize atom positions, it is useful to examine specific crystallographic planes. Figure 1.14 shows the (110) plane of the rocksalt structure, in which the row of cations corresponds to a row of octahedral sites at one-half the unit cell height. In this plane also lies unoccupied tetrahedral sites at heights of 1/4 and 3/4a_o, which may be visualized by referring back to Figure 1.8. Note that simultaneous occupation of the octahedral and tetrahedral sites would bring two cations into close proximity with no shielding anions in between; this is an electrostatically unfavorable arrangement that is avoided. In structures that do have both octahedral and tetrahedral sites occupied, such as the spinel structure discussed below, partial occupancy of each type of site allows cations to be arranged in a way that avoids this like-neighbor repulsion. In Fig. 1.14, the close-packed

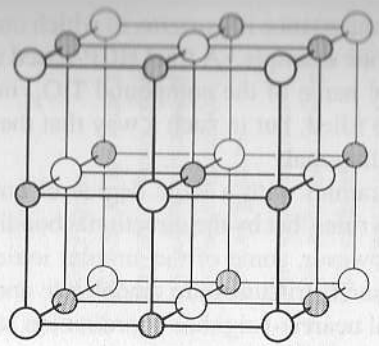

(a)

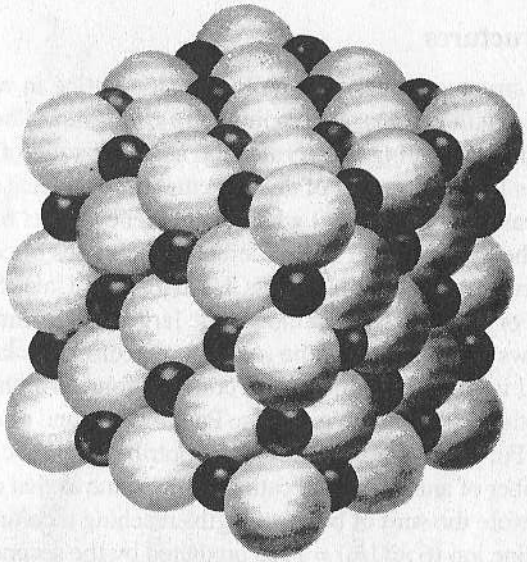

(b)

Fig. 1.13 Crystal structure of sodium chloride.

direction shown is the shortest distance between anions and lies in the close-packed plane, which for FCC is the (111) plane (shown earlier in Figs. 1.1 and 1.3). Note that neither the octahedral nor tetrahedral sites lie exactly in this plane since interstitial sites are formed *between* close-packed planes. Parallel to the close-packed anion planes exist alternating layers of similarly packed cations fully occupying the octahedral sites. We thus observe that between any two close-packed layers of anions in the rocksalt structure, there lies a hexagonal array of cations with an identical periodicity.

Antifluorite and Fluorite. What kinds of compounds can be based on FCC anion packing with all of the tetrahedral sites filled? Since there are twice as many

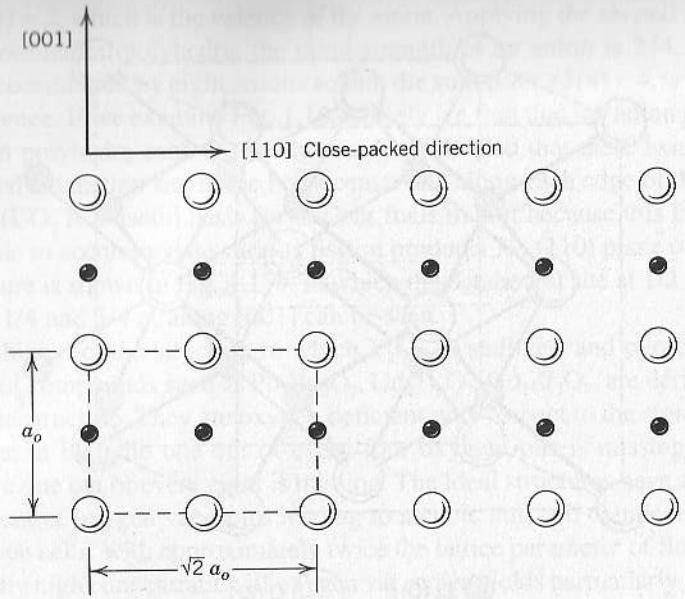

Fig. 1.14 (110) plane of the rock salt structure.

tetrahedral sites as atoms, the stoichiometry must be M_2X. Examples include the alkaline oxides such as Li_2O, Na_2O, and K_2O. They crystallize in the *antifluorite* structure, which is the structural counterpart to the fluorite structure but with the cation and anion positions reversed and a stoichiometry of MX_2. Figure 1.15*a* shows one unit cell of the antifluorite structure compound Li_2O, in which all tetrahedral sites are occupied by the alkali ion.

The Li ions are somewhat larger than we would expect to find in the tetrahedral sites according to Pauling's first rule, but there are too many for the available octahedral sites, so occupying the tetrahedral sites is the next best thing. The bond strength is 1/4, so according to the second rule the coordination of Li^{1+} ions around each oxygen must be eight. If we examine Fig. 1.15*a*, this coordination can be verified. The connectivity of the tetrahedra is completely edge sharing; each tetrahedron shares two of its oxygen ions with a neighboring tetrahedron.

The fluorite structure is named for the mineral fluorite, CaF_2. Oxides of the fluorite structure, particularly ZrO_2, UO_2, and CeO_2, have great technological importance in structural, electrical, and chemical applications. It is a common structure for binary compunds in which the cation is large enough that eight-fold coordination is preferred. The structure is based on FCC close-packing of the cations with all tetrahedral interstices filled by anions. We can envision it simply by reversing the cation and anion positions in Fig. 1.15*a*. The coordination of cations around anions is 4. Using ZrO_2 as an example, if we apply Pauling's second rule to the anion polyhedra as above, the bond strength contributed by each cation is 4/8. Since there are four cations surrounding each anion, the sum of bond strengths

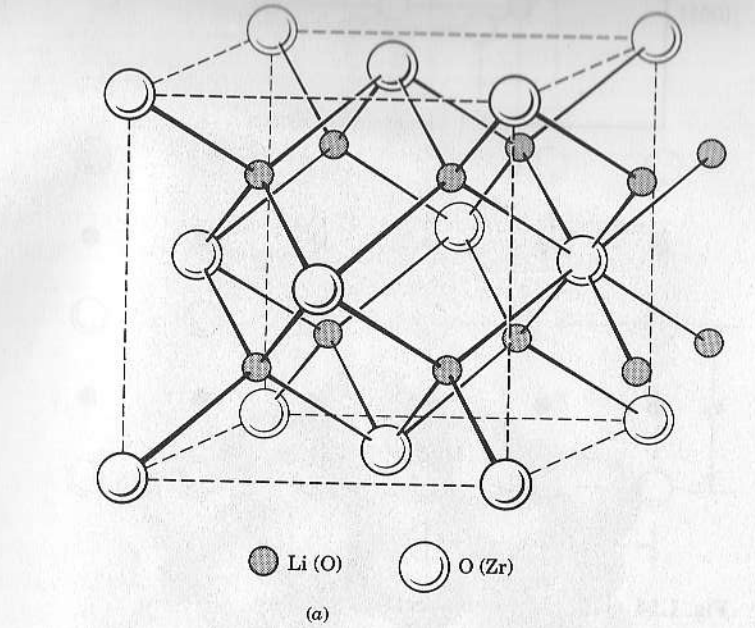

Fig. 1.15 (*a*) Antifluorite (fluorite) structure, typified by compounds Li_2O and ZrO_2. (*b*) (110) plane of the fluorite structure compound ZrO_2.

is $4 \times (4/8) = 2$, which is the valence of the anion. Applying the second rule to the cation coordination polyhedra, the bond strength of an anion is 2/4, and each cation is coordinated by eight anions so that the sum is $8 \times (2/4) = 4$, which is the cation valence. If we examine Fig. 1.16a closely we find that the anion polyhedra and cation polyhedra each share edges only. Note also that there exists a large unoccupied octahedral site in the body-center and along each edge of the fluorite unit cell. (UO_2 is a useful basis for nuclear fuels in part because this large interstice is able to accommodate various fission products.) A (110) plane of the fluorite structure is shown in Fig. 1.15*b*, in which the octahedral site at 1/2 a_0 and the anions at 1/4 and 3/4 a_0 along [001] can be seen.

Cubic bixbyite, the structure in which Y_2O_3 crystallizes, and pyrochlore, the structure of compounds such as $Pb_2Ru_2O_7$, $Gd_2Ti_2O_7$, $Gd_2Zr_2O_7$, are derivatives of the fluorite structure. They are oxygen deficient with respect to the stoichiometry of fluorite; in bixbyite one out of every four oxygen ions is missing, while in pyrochlore one out of every eight is missing. The ideal structures have an ordered arrangement of oxygen vacancies leading to a cubic unit cell composed of eight fluorite type cells, with approximately twice the lattice parameter of flourite. The intrinsically high concentration of oxygen vacancies yields particularly good oxygen ion conduction in some pyrochlores. The FCC cation sublattice is also ordered in the ideal pyrochlore structure. Disorder on both the cation and anion sublattices is possible at elevated temperatures, and further increases the ionic conductivity.

Zincblende. Oxides and sulfides (such as ZnO, ZnS, BeO) with smaller cations that prefer tetrahedral coordination tend to form this structure, as well as covalent compounds such as SiC, BN, and GaAs (for reasons discussed as follows). It is named after the mineral zincblende, ZnS. In contrast to the rocksalt structure in which all octahedral sites were filled, here we need only fill one-half of the tetrahedral sites with the divalent cation in order to satisfy the MX stoichiometry. Recalling from Fig. 1.8*b* that the tetrahedral sites in FCC form a primitive cubic array, we can fill half of them on the opposing corners of the cube in order to achieve maximum cation separation. The resulting structure is shown in Fig. 1.16. With four anions coordinating each cation the bond strength is 2/4. We also see that each anion is coordinated by four cations; hence, the sum of bond strengths to the anion is 2 and satisfies the second rule. The anion coordination tetrahedra share only corners in this structure.

A number of covalent compounds crystallize in the zincblende structure, but for quite different reasons than the electrostatic arguments embodied in Pauling's rules. Zincblende is one structure type of SiC (others are discussed in the special topic *Polymorphs and Polytypes*), because the covalent bond between Si and C results from the overlap of sp^3 hybridized orbitals with tetragonal directionality. Since atoms of both types are tetrahedrally coordinated in the zincblende structure, this need is mutually satisfied. This tendency is also shared by III-V semiconductor compounds such as GaAs, CdS, GaP, and InSb. For these covalently

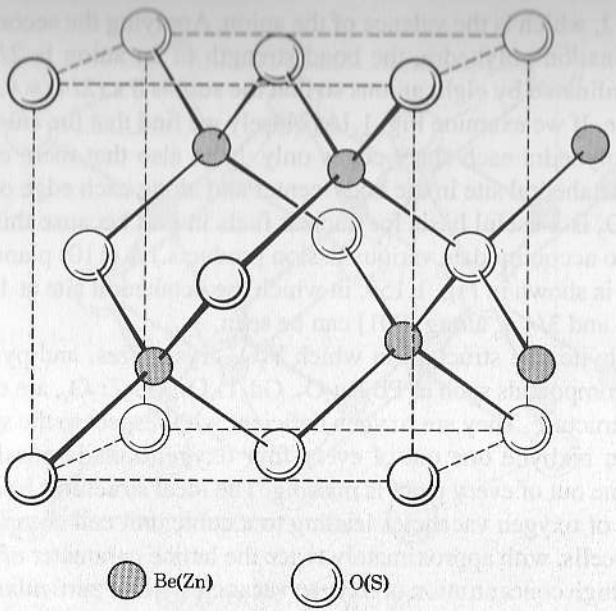

Fig. 1.16 Zincblende (ZnS) structure.

bonded binary compounds the zincblende structure can be viewed as a derivative of the simpler diamond cubic structure. If all atoms in the zincblende structure are identical, we obtain the diamond cubic structure (Fig. 1.17), which is the crystalline form of this well-known phase of carbon as well as that of silicon and germanium. All three are covalent elemental semiconductors with sp^3 hybridized orbital covalent bonding.

Many compounds of zincblende structure can also crystallize in the *wurtzite* structure, discussed in the next section, which shares identical coordination num-

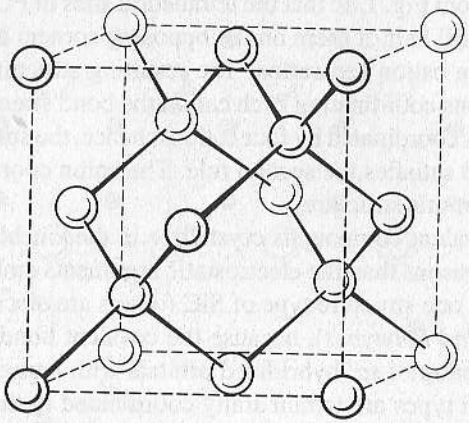

Fig. 1.17 Crystal structure of diamond.

bers. For ionic compounds, the electrostatic energy difference (Madelung constant, Table 1.1) between these two structures is very small; hence, there is little preference to form one over the other. Since the two differ only in the stacking sequence of a two-dimensional layer, they may also be considered polytypes of one another.

SPECIAL TOPIC 1.1

POLYMORPHS AND POLYTYPES

Although we discussed ZrO_2 as a *cubic* fluorite structure, in reality there are three distinct crystalline forms or *polymorphs* of this one compound. These are the cubic, tetragonal, and monoclinic phases (Fig. ST1), in which the crystal symmetry differs, as do the detailed interatomic spacings, but the numerical coordination of ions does not. Transformations between the different phases in this system can occur by simple atom displacements, and are known as *displacive* transformations. Other phase transformations require bond breaking and rearrangement, and are known as *reconstructive* transformations.

Cubic ZrO_2 is the highest temperature phase, only stable in the pure form at temperatures between ~2370°C and the melting point at ~2680°C, as shown in the phase diagram in Fig. ST1. However, upon the addition of a few percent of "stabilizers," such as CaO, MgO, or Y_2O_3, this cubic phase can be preserved to lower temperatures (Fig ST1). While the region of thermodynamic stability (equilibrium single phase field) does not reach room temperature for cubic ZrO_2-MgO or other stabilizers (see the ZrO_2-CaO diagram in Fig. 4.8), it can be retained upon cooling as a metastable phase. The cubic forms of ZrO_2–CaO and ZrO_2–Y_2O_3 are technologically important as

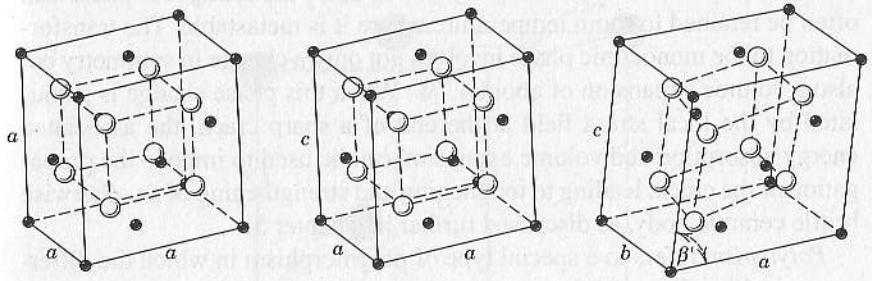

Fig. ST1 Three polymorphs of ZrO_2: (*a*) c phase, (*b*) t phase (c/a ~1.02), (*c*) m phase. (From A. H. Heuer and M. Rühle, "Phase Transformations in ZrO_2-Containing Ceramics: I, The Instability of c-ZrO_2 and the Resulting Diffusion-Controlled Reactions," *Advances in Ceramics*, Vol. 12, *Science and Technology of Zirconia II*, Nils Claussen, M. Rühle, and A. H. Heuer, Eds., The American Ceramic Society, 1984.)

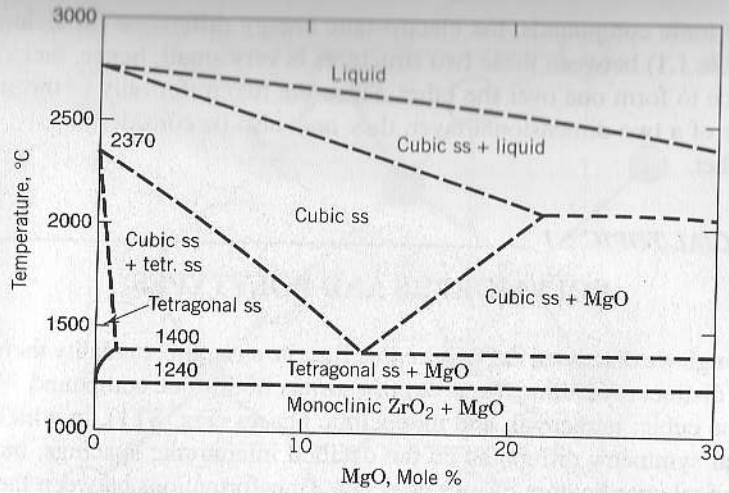

Fig. ST2 Phase diagram of the ZrO_2-rich region in the MgO-ZrO_2 binary system. (From S. C. Farmer, T. E. Mitchell, and A. H. Heuer, "Diffusional Decomposition of c-ZrO_2 in Mg-PSZ," *Advances in Ceramics*, Vol. 12, *Science and Technology of Zirconia II*, N. Claussen, M. Rühle, and A. H. Heuer, Eds., The American Ceramic Society, 1984.)

oxygen ion conductors used in sensors and fuel cells, and as diamond substitutes in the gem trade. The tetragonal-to-monoclinic phase transformation is important for structural applications since it is the basis for *transformation toughening*. While Fig. ST2 shows this transformation occuring at ~1240°C in pure zirconia, in lightly doped ZrO_2 the tetragonal phase can often be retained to room temperature where it is metastable. The transformation to the monoclinic phase involves not only a change in symmetry but also a volume expansion of about 4.7%. When this phase change is stimulated by the local stress field at the end of a sharp crack, the associated energy absorption and volume expansion can be used to impede the propagation of the crack, leading to toughening and strengthening of an otherwise brittle ceramic body, as discussed further in Chapter 5.

Polytypism refers to a special type of polymorphism in which the different crystalline forms of the compound are related by different stacking sequences of a two-dimensional layer. One example is the zincblende and wurtzite structures, which differ only in the stacking sequence of tetrahedrally filled close-packed anion layers. Note that the transformation between the two is necessarily reconstructive, and requires atom diffusion unlike a displacive transformation such as that in zirconia. Another example of a polytypic material is silicon carbide, which can form in not only the zincblende

and wurtzite structures but also in a wide variety of stacking sequences with larger periodicity (more than 74 different polytypes have been identified). One reasonably stable polytype is called "6H" (in what is known as Ramsdell notation) because it requires six close-packed layers to repeat the stacking sequence, and the resulting symmetry is hexagonal. According to this notation, cubic or "β" SiC is called "3C," signifying a three-layer stacking sequence and cubic symmetry, while "2H" is the polytype corresponding to wurtzite. "15R" is another type, which repeats after 15 layers and is rhombohedral in symmetry. By convention, all SiC polytypes other than 3C are generally considered to be "α" silicon carbide.

HCP-Based Structures

Wurtzite. The wurtzite structure is based on the HCP close-packing of anions, with one-half of the tetrahedral sites occupied by the cations. The coordination number of each ion is 4. Let's examine the spatial distribution of tetrahedral sites in HCP to determine how they can be one-half filled, with maximum separation between cations. We earlier showed that there are two orientations of tetrahedral sites between close-packed anion layers: those with the apex "up" and those with the apex "down" (Figs. 1.7 and 1.9). Examining Fig. 1.7 closely, it can be seen that there are equal numbers of each, and that each forms a hexagonal array with the same spacing as the anions. One can therefore fill one-half the total tetrahedral sites with maximum separation by filling only tetrahedra of one orientation. This is shown in the unit cell for the wurtzite structure in Fig. 1.18, where all of the filled tetrahedral sites have their apex upward. The coordination of anions around

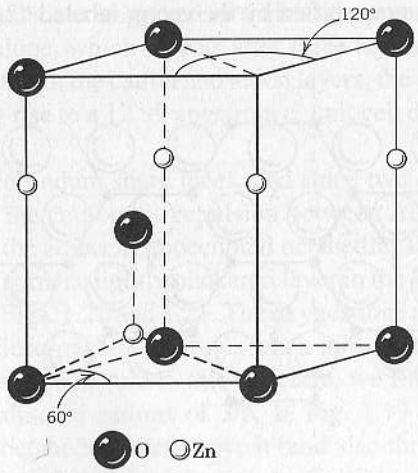

Fig. 1.18 Unit cell of the wurtzite structure.

cations and of cations around anions is four, as in the zincblende structure, thus we can be satisfied that the wurtzite structure also meets the requirements of Pauling's second rule. The unit cell for wurtzite is smaller than that of zincblende (it contains only two MX formula units rather than four), so it is more difficult to visualize the interconnections between tetrahedra; they are also linked by corners. We mentioned previously that the Madelung constants of the zincblende and wurtzite structures are very similar (1.638 and 1.641, respectively). Since each has one-half of the tetrahedral sites filled as well it is reasonable that compounds of one structure often have a polytype of the other. Furthermore, since both atoms are tetrahedrally coordinated in wurtzite, it, like zincblende, is the preferred structure of a number of covalent compounds, including AlN and the α phases of SiC.

Corundum. The corundum structure is named for the compound Al_2O_3, also commonly referred to as aluminum oxide, α-alumina (several other polymorphs exist), or sapphire (which commonly refers to the single crystalline form, as it is the basis of ruby, blue sapphires, and star sapphires). Other compounds of corundum structure include Fe_2O_3 and Cr_2O_3. The ilmenite ($FeTiO_3$) and lithium niobate ($LiNbO_3$) structures discussed below are derivatives of corundum. Based on the 2:3 cation:anion stoichiometry of these compounds, cations that take on octahedral coordination must fill two-thirds of the available sites. To see how this occurs in an orderly way with maximum cation separation, the location of octahedral sites between two layers of close-packed oxygen ions have been drawn in Fig. 1.19 (only one oxygen layer is shown). These octahedral sites form a hexagonal array with the same spacing as the oxygen layers. We show the two-thirds that are occupied by aluminum ions in corundum with filled circles, and the one-third remaining empty octahedral sites with x's. The next cation layer has the same honeycomb configuration but is shifted by one atomic spacing, in the direction of the vector labeled "1" in Fig. 1.19. After another close-packed oxygen layer, a third cation layer is placed, now shifted by the vector labeled "2." If we take a vertical

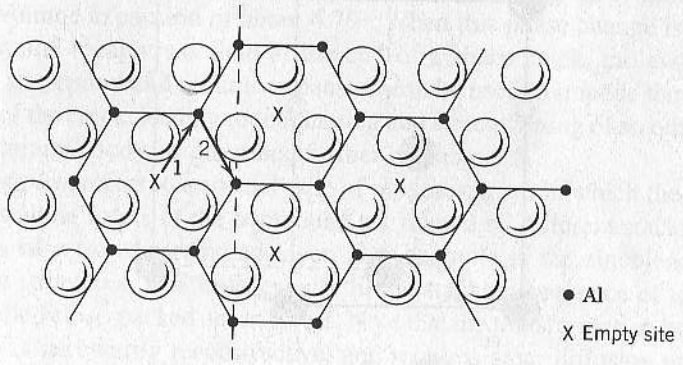

Fig. 1.19 Filling of 2/3 of the octahedral sites in the basal plane of corundum. Only one close-packed anion plane is shown.

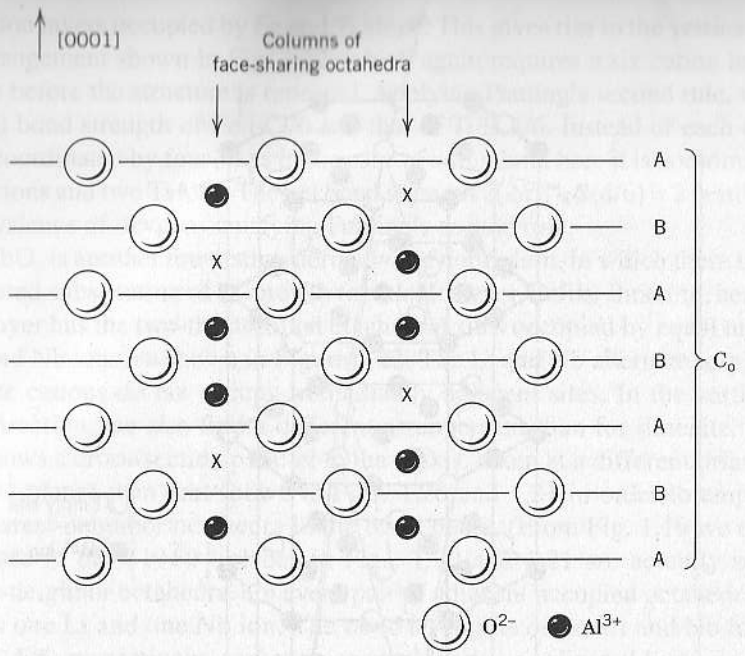

Fig. 1.20 Plane shown by dashed line in Fig. 1.19. Two-thirds occupancy of the columns of octahedral sites is shown.

slice (normal to the plane of the paper) as indicated by the dashed line in Figure 1.19, we have a plane of $\{10\bar{1}0\}$ type in which the arrangements of ions are as shown in Figure 1.20. The columns of octahedral sites perpendicular to the (0001) or basal plane of corundum alternate in having every two sites occupied and one empty. Adjacent columns are staggered in their site occupancy. Fig. 1.21 shows the cation sublattice alone, which repeats after three layers. Taking into account the periodic spacing of both the cation and anion layers, the structure repeats itself after six layers, giving rise to a 12.99 angstrom c_0 unit cell dimension as shown in Fig. 1.20 and 1.21.

The octahedra in corundum share faces, and since two out of every three are occupied (Fig. 1.20), the coulombic repulsion between Al^{3+} ions causes each to move slightly toward the adjacent unoccupied octahedral site. As a result, in real corundum the cations form a slightly puckered layer in the basal plane rather than the ideal structures in Figs. 1.20 and 1.21. The oxygen ions also shift slightly from idealized hexagonal close-packed positions when this occurs.

Applying Pauling's second rule to this structure, we find a bond strength for the octahedrally coordinated cations of 3/6. In Fig. 1.19 we can see that each oxygen ion has three octahedral sites above it (and also three below). Since only two of the three are occupied, the total number of cations around oxygen is four. This satisfies the second rule since the sum is 4(3/6) = 2.

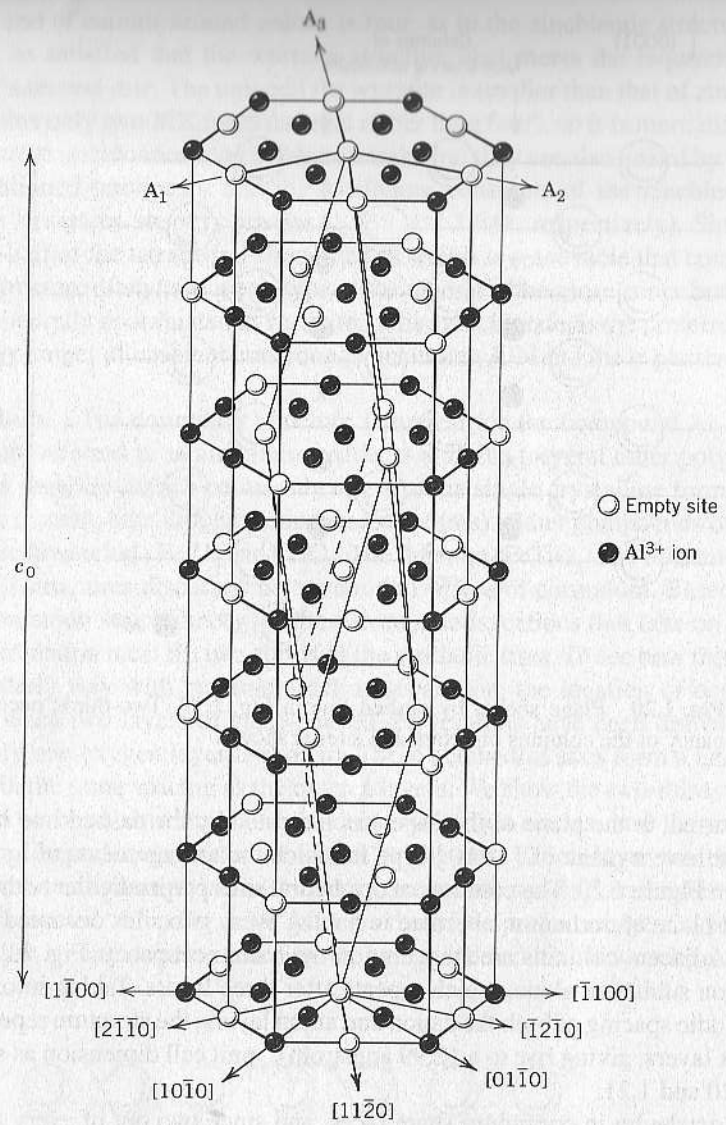

Fig. 1.21 Structural unit cell of corundum (Al_2O_3), showing only the cation sublattice. A_1's are the hexagonal basis vectors.

Ilmenite and Lithium Niobate. Two structures that directly follow from the corundum structure are ilmenite and lithium niobate. Ilmenite is the compound $FeTiO_3$; other ABO_3 compounds in which A and B both prefer octahedral coordination can also take on this structure. As in corundum, two-thirds of the octahedral sites are filled, in this case by an ordered substitution of Fe and Ti for Al. The two-thirds-filled arrangement shown in Fig. 1.20 is preserved, but with alternating cation layers occupied by Fe and Ti alone. This gives rise to the vertical stacking arrangement shown in Fig. 1.22, which again requires a six cation layer sequence before the structure is repeated. Applying Pauling's second rule, we find that the bond strength of Fe is 2/6 and that of Ti is 4/6. Instead of each oxygen being coordinated by four Al as in the case of corundum, here it is coordinated by two Fe ions and two Ti ions. The net bond strength 2(2/6) + 2(4/6) = 2 is still equal to the valence of oxygen, satisfying Pauling's second rule.

$LiNbO_3$ is another interesting derivative of corundum, in which there is again an ordered substitution of Li and Nb for Al. However, unlike ilmenite, here each basal layer has the two-thirds-filled octahedral sites occupied by equal numbers of Li and Nb ions, as shown in Figure 1.23. The Li and Nb alternate in-plane so that like cations do not occupy immediately adjacent sites. In the vertical (c-axis) direction, we also find a different arrangement than for ilmenite. Figure 1.24 shows a cross-section parallel to the c-axis, taken at a different orientation ($\{11\bar{2}0\}$ plane) than that shown in Figs. 1.20 and 1.21 in order to emphasize first nearest-neighbor octahedra in the basal plane. (From Fig. 1.19 we can see that those in the $\{10\bar{1}0\}$ planes in Figs. 1.20 and 1.21 are actually second-nearest-neighbor octahedra.) In every pair of adjacent occupied octahedral sites there is one Li and one Nb ion. The bond strengths of the Li and Nb ions are 1/6 and 5/6, respectively, and each oxygen ion is coordinated by two of each type, satisfying the second rule.

Notice that each of the Li-Nb pairs in Figure 1.24 is oriented in the same direction, unlike ilmenite in which the Fe-Ti pairs alternate direction. Due to the charge

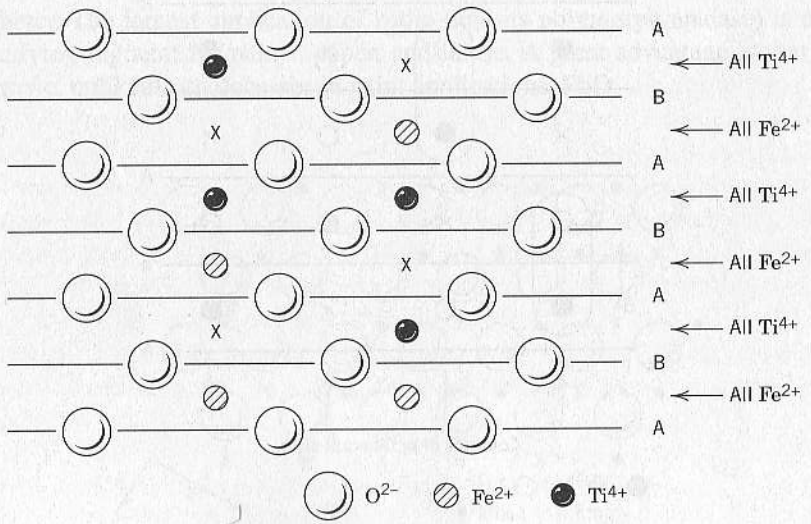

Fig. 1.22 Ilmenite structure in same projection as Fig. 1.20.

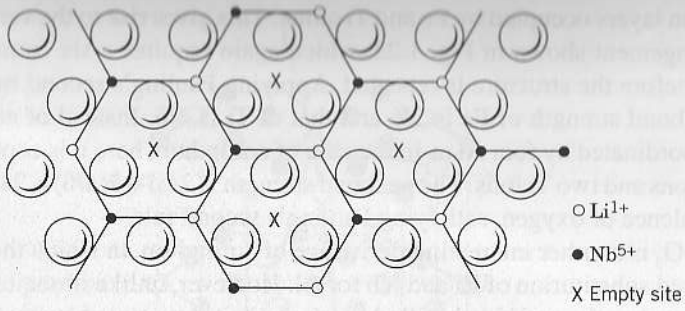

Fig. 1.23 Basal plane of $LiNbO_3$ structure, showing mixed Li, Nb occupancy.

distribution between the Li-Nb pair, a net electric dipole exists for each of the pairs in the structure. This yields a ferroelectric crystal with a permanent net polarization. The anisotropy in structure also yields a highly anisotropic refractive index (birefringence), which is furthermore responsive to applied electric field (high electro-optical coefficients). Because of these properties, lithium niobate has been a leading candidate material for electro-optic devices.

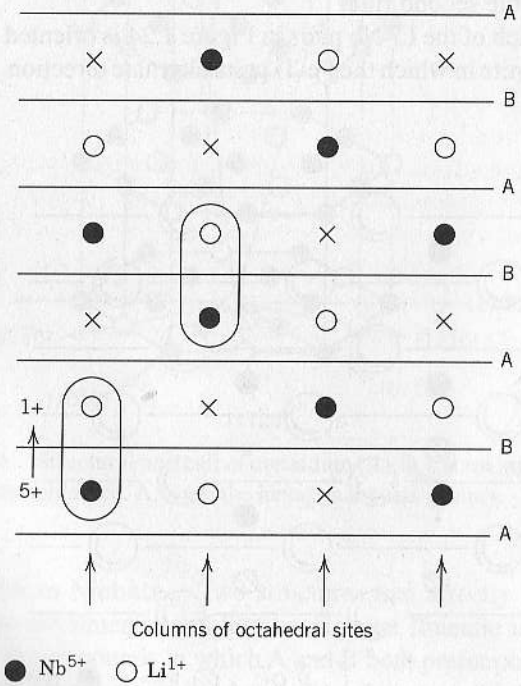

Fig. 1.24 Cation arrangement in $LiNbO_3$, showing orientation of dipole between Li^{1+} and Nb^{5+}.

Rutile. Rutile is one polymorph of the mineral TiO_2 (anatase and brookite are the others) and has a structure based on quasi-HCP packing of oxygen atoms. Although the cations fill one-half of the available octahedral sites in HCP, the resulting unit cell is tetragonal. We will show how this unit cell arises.

Beginning again with a close-packed oxygen plane and the octahedral sites that exist between it and the next oxygen layer, we can fill one-half of the octahedral sites by completely filling alternating diagonal rows, as shown in Fig. 1.25. Any horizontal row then obviously has one-half of the octahedral sites filled. The next layer of octahedral sites lies directly above the octahedral sites shown here (since the stacking is HCP). In this layer, the Ti atoms fill sites that are directly above the empty ones shown here, and the empty sites are directly above filled ones. The third cation layer is directly above the first one, so that the ABA stacking sequence is simply repeated. The resulting unit cell is tetragonal. However, the atoms do relax from their positions in the perfect HCP lattice due to the partial occupancy of sites by the highly charged Ti^{4+} ions. The dotted line in Fig. 1.25 outlines one side of the unit cell, shown in its usual tetragonal perspective in Fig. 1.26. The octahedron of oxygen ions in Fig. 1.26 comes from two close-packed layers of the type in Fig. 1.25. Comparing these two figures, it is possible to see that the tetragonal structure then has columns of filled octahedral sites along the c-axis direction, and a similar parallel column of empty octahedral sites. This site arrangement results in very anisotropic diffusion properties for some cations in rutile structure oxides. Small cations in particular are able to diffuse interstitially through the empty octahedral sites, and therefore diffuse much faster along the c-axis direction than in the a-axis direction.

Rutile TiO_2 has a large and highly anisotropic refractive index (high birefringence), and has great scattering power as a fine powder of a few tenths of a micron diameter. The largest application of rutile (and its polymorph anatase) is as an opacifying pigment for paints, paper, and fabric. A great advantage is that it is nontoxic, unlike its predecessor in paint applications, PbO.

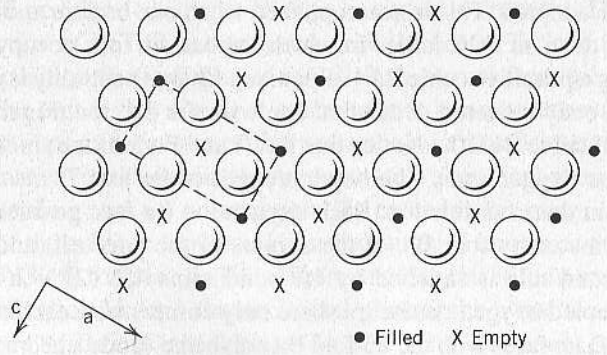

Fig. 1.25 One-half filling of octahedral sites in a close-packed plane (rutile structure).

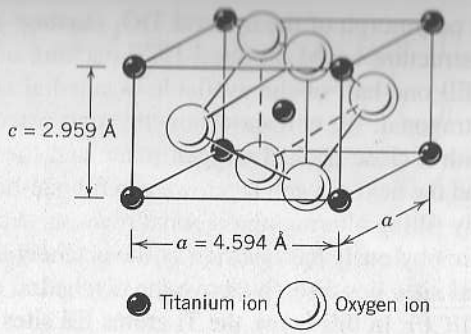

Fig. 1.26 Unit cell of rutile structure.

Perovskite

Many ternary compounds of formula ABO_3 for which the A and B cations differ considerably in size crystallize in the perovskite structure. While no one sublattice is actually close-packed, the structure can be considered an FCC-derivative structure in which the larger A cation and oxygen together form an FCC lattice. The smaller B cation occupies the octahedral sites in this FCC array and has only oxygen as its nearest neighbors. The perovskite family includes many titanates used in electroceramic applications, such as $BaTiO_3$, $CaTiO_3$ (which is the mineral perovskite), $SrTiO_3$, and $PbTiO_3$, zirconates such as $PbZrO_3$ and $BaZrO_3$, and a number of other compounds including $LaGaO_3$, $LaAlO_3$, and $KNbO_3$. It is also a partial structural unit in some more complex structures, such as the superconducting cuprates. For the present discussion, we will use the high-temperature cubic form of $BaTiO_3$ as our model perovskite.

The radius ratio expected for Ba^{2+} to O^{2-} is large, ranging from 0.96 to 1.15 depending on the coordination number we choose (Table 1.2). Although this ratio would appear to be too large for octahedral coordination, the binary compound BaO nonetheless forms in the rocksalt structure since the stoichiometry requires a 1:1 site-to-atom ratio. In $BaTiO_3$, however, a more favorable 12-fold coordination of Ba^{2+} can be adopted. This is accomplished when one barium and three oxygen ions together form an FCC lattice in which the barium ions occupy corner positions (forming a primitive cubic Ba^{2+} sublattice). Charge neutrality is accomplished by filling the body-centered octahedral site with the Ti^{4+} ion. Figure 1.27 shows the unit cell of cubic $BaTiO_3$. Notice that the Ti and Ba ions are shielded from one another by the oxygen ions. The bond strength of Ba and Ti are 2/12 and 4/6, respectively, in this coordination. Each oxygen ion (in face positions on the unit cell) is coordinated by four Ba (at the corners of the unit cell) and two Ti ions. Pauling's second rule is satisfied by the bond sums 4(2/12) + 2(4/6) = 2. The titanium-occupied oxygen octahedra share only corners with each other, but they unavoidably share faces with the 12-fold Ba polyhedra (dodecahedra). It is difficult to imagine a simpler way of accommodating two cations that are very different in size. Perovskites can be of $A^{2+}B^{4+}O_3$ stoichiometry, as in $BaTiO_3$ and $PbZrO_3$, or

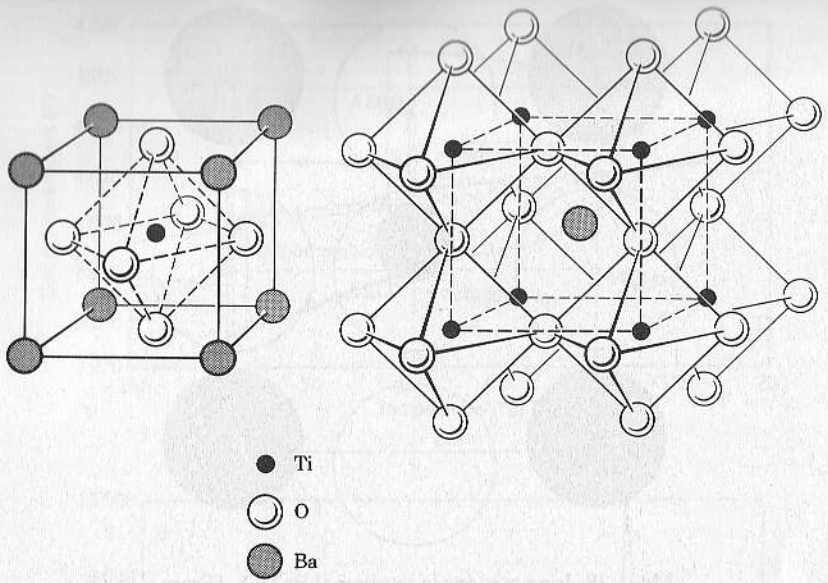

Fig. 1.27 Ion positions in ideal cubic perovskite structure.

$A^{3+}B^{3+}O_3$ stoichiometry, as in $LaGaO_3$ and $LaAlO_3$. Mixed $A(B^{2+}_{1/3}B^{5+}_{2/3})O_3$ or $A^{2+}(B^{3+}_{1/2}B^{5+}_{1/2})O_3$ compositions are also possible, as in $Pb(Mg_{1/2}Nb_{2/3})O_3$ and $Pb(Sc_{1/2}Ta_{1/2})O_3$. In each instance the A-site cations are the larger. An enormous range of perovskite compositions and solid solutions have been developed for technical applications.

Like ZrO_2, many perovskite compounds exist in polymorphs of different crystal symmetry related by simple displacive transformations. The most important of these is the cubic-to-tetragonal transformation. In $BaTiO_3$, the oxygen octahedron coordinating Ti is larger than necessary, being expanded by the large Ba nearest neighbors. This causes the Ti ion to be somewhat unstable in the sense described by Pauling's first rule. The "rattling titanium" ion can be easily displaced from the body-centered position, causing a change in crystal symmetry. The room-temperature structure of $BaTiO_3$ is tetragonal, with the center Ti^{4+} occupying a minimum energy position that is displaced by ~0.12 angstroms from the center toward one face of the unit cell, yielding a structure that is noncentrosymmetric (Fig. 1.28). A most important feature of this spontaneous transformation is that it results in a permanent electrical dipole. A cooperative alignment of adjacent dipoles then occurs, leading to a net polarization that extends over many unit cells. The temperature of the cubic to tetragonal transformation is known as the Curie point and occurs at 130°C for pure $BaTiO_3$. There are also lower temperature transformations to orthorhombic and rhombohedral phases; the transitions between the different phases of $BaTiO_3$ are depicted in Fig. 1.29. The phase transformation temperatures vary widely among perovskites. In $PbTiO_3$, which has a larger Pb^{2+} ion in place of Ba^{2+} and a still more unstable octahedral environment for Ti^{4+}, the

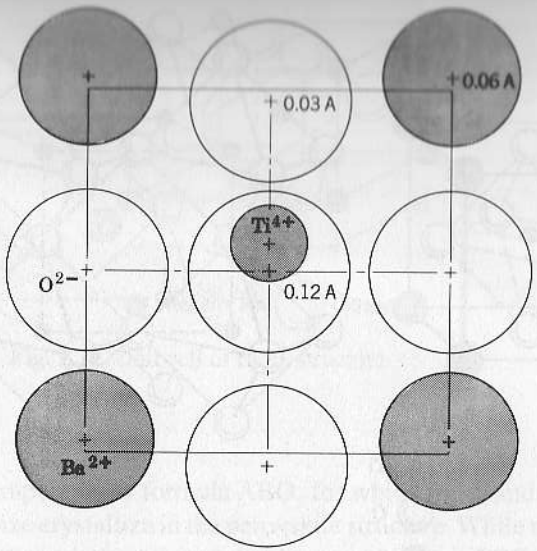

Fig. 1.28 Ion positions in tetragonal $BaTiO_3$. [From G. Shirane, F. Jona, and R. Pepinsky, *Proc. I.R.E.*, 42, 1738 (1955).]

cubic to tetragonal transformation occurs at a higher temperature (490°C) than in $BaTiO_3$. Conversely, $SrTiO_3$ has its Curie point at a lower temperature of -55°C. This can be rationalized from the point of view that the smaller ionic size of Sr^{2+} results in a smaller oxygen octahedron than in $BaTiO_3$, which stabilizes the Ti ion in its centralized position. In practice the Curie point can be continuously varied over a wide range by forming solid solutions between $BaTiO_3$ and $PbTiO_3$ (to raise T_c) or $SrTiO_3$ (to lower T_c).

Perovskite-based compounds are the basis for a large fraction of the existing electronic, electro-optical, and electromechanical applications of ceramics. In almost every instance, the property of interest is derived from the spontaneous or field-assisted electrical polarization of the noncubic forms. The existence of a permanent electrical dipole allows coupling between an applied electric field and the dielectric, mechanical, or optical properties of the crystal. During the cubic-to-tetragonal transformation, the unstable central titanium ion is easily displaced in one of the six [001] directions by an external electric field; the material can be "poled." In some capacitor applications of perovskites, the orientation of an impending polarization yields unusually high effective dielectric constants. Also accompanying the transformation is a change in crystal dimensions. The coupling between crystal dimensions and applied field is the origin of the *piezoelectric* effect, useful in electromechanical applications where electrical energy is converted to mechanical energy, or vice versa. Lead titanate–lead zirconate solid solutions (given the acronym PZT) have been developed as piezoelectrics for such applications as speakers and microphones, sonar transducers, ultrasonic cleaners, and actuators for high-precision positioning. Anisotropy in the optical refractive index (birefringence) also accompanies the electric polarization. The switchable birefringence of ferroelectric perovskites such as La-substituted $PbTiO_3$-$PbZrO_3$ (PLZT) enables applications such as optical shutters, displays, and optical memory. Another application that utilizes the ferroelectric transition is the $BaTiO_3$ positive-temperature-coefficient (PTC) resistor, in which the spontaneous polarization upon cooling below the Curie temperature causes the removal of grain boundary barriers to conduction, resulting in enormous changes in resistivity. PTC resistors are used as temperature sensors and as self-regulating heating elements, discussed further in Chapter 3.

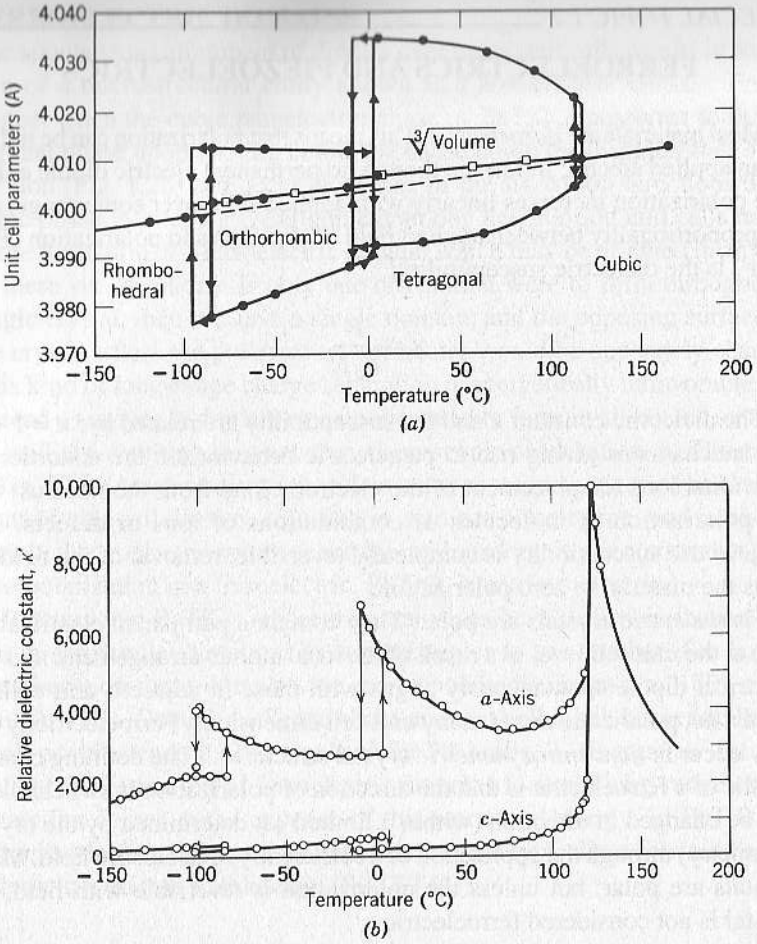

Fig. 1.29 (*a*) Dimensions of pseudocubic unit cell of $BaTiO_3$. [From H. F. Kay and P. Vousdan, *Phil. Mag.*, 7, 40, 1019 (1949).] (*b*) Temperature dependence of dielectric constant. [From W. J. Merz, *Phys. Rev.*, 76, 1221 (1949).]

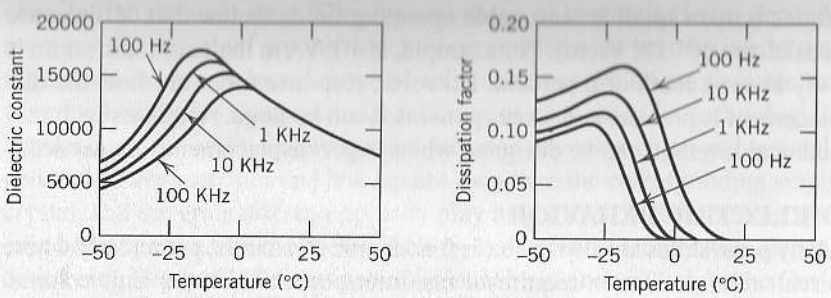

Fig. ST8 (*a*) Dielectric constant and (*b*) loss factor as a function of temperature and frequency for lead magnesium niobate (PMN) relaxor ferroelectric. [From S.L. Swartz, T. R. Shrout, W. A. Schulze, and L. E. Cross, *J. Am. Ceram. Soc.*, 67[5] 311 (1984).]

Relaxor ferroelectrics (sometimes *relaxator*), of which $Pb(Mg_{1/3}Nb_{2/3})O_3$ is an example, are also based on the perovskite structure but with an ordering of the B-site cations that requires eight perovskite units to form a unit cell (Fig. ST7). This ordering occurs over a broad range of temperature as a *diffuse phase transition* occurring in microdomains of the crystal, rather than as a single sharp phase transition at the Curie point. The resulting dielectric constant shows a broad peak with values as high as 25,000 ε_o over

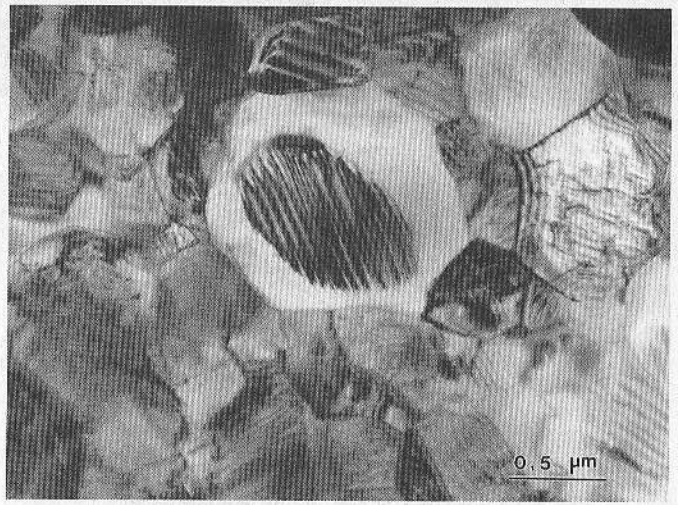

Fig. ST9 Transmission electron microscope view of core-shell structure in a $BaTiO_3$ X7R type capacitor material. (Courtesy of Masayuki Fujimoto, Taiyo Yuden Co., Ltd., Gunma, Japan.)

the temperature range where B-site cation ordering takes place (Fig. ST8). Hysteresis is small in the absence of conventional ferroelectric domains.

Another means of achieving temperature stability of capacitance in a ferroelectric is to incorporate a range of compositions and therefore a range of Curie points in a single material. This is the principle behind so-called "X7R" dielectrics (named after an technical specification, not a material!) which require that the dielectric constant vary by no more than +15% over the temperature range of -55°C to +125°C. These are based on polycrystalline $BaTiO_3$ into which dopants such as Bi and Nb have been diffused along grain boundaries to create a "shell" in each grain of lower Curie point and a lesser-doped "core" of higher Curie point. Figure ST9 shows a room-temperature transmission electron microscope image of this core-shell structure, where the undoped center has undergone its ferroelectric transition and shows a domain structure. This process in effect creates a composite dielectric structure and broadens the Curie transition; the dielectric constant is typically 3000-5000 ε_o. Barrier layer capacitors are another type of dielectric based on polycrystalline $SrTiO_3$ or $BaTiO_3$ in which the grains are conductive but the grain boundaries insulating. These materials utilize space-charge polarization within each grain in addition to an intrinsically high dielectric constant to achieve dielectric constants that can exceed 20,000 ε_o.

Spinel

The spinel structure is based on an FCC close-packed oxygen sublattice in which a fraction of the octahedral and tetrahedral sites are filled. Compounds of stoichiometry AB_2O_4 in which the cations A and B are divalent and trivalent, respectively, ($AO \cdot B_2O_3$) often form as spinels. The unit cell of spinel contains eight FCC oxygen subcells in a cubic array. One-half of the octahedral sites and one-eighth of the tetrahedral sites are occupied. In a *normal* spinel, such as $MgAl_2O_4$ (the mineral spinel), the B^{3+} cations occupy one-half of the octahedral sites and the A^{2+} cations one-eighth of the tetrahedral sites. The A^{2+} bond strength is therefore 2/4 and the B^{3+} bond strength 3/6. In order to satisfy the second rule each oxygen must be coordinated by three octahedral cations and one tetrahedral cation. This structure is shown in Fig. 1.31 as sequential atomic layers parallel to the (100) plane of the unit cell, at height increments of 1/8 a_o. Figure 1.30 shows a three-dimensional depiction. An *inverse* spinel $B(AB)O_4$ has a slightly different occupancy, in which one half of the B^{3+} cations occupy the one-eighth-filled tetrahedral sites, and the A^{2+} ions and the remaining half of the B^{3+} ions occupy octahedral positions. The occupied sites remain those shown in Fig. 1.30, but the cations are exchanged. In reality, most spinels whether they are normal or inverse are disordered to some degree by exchange of the A^{2+} and B^{3+} cations. They may be thought of

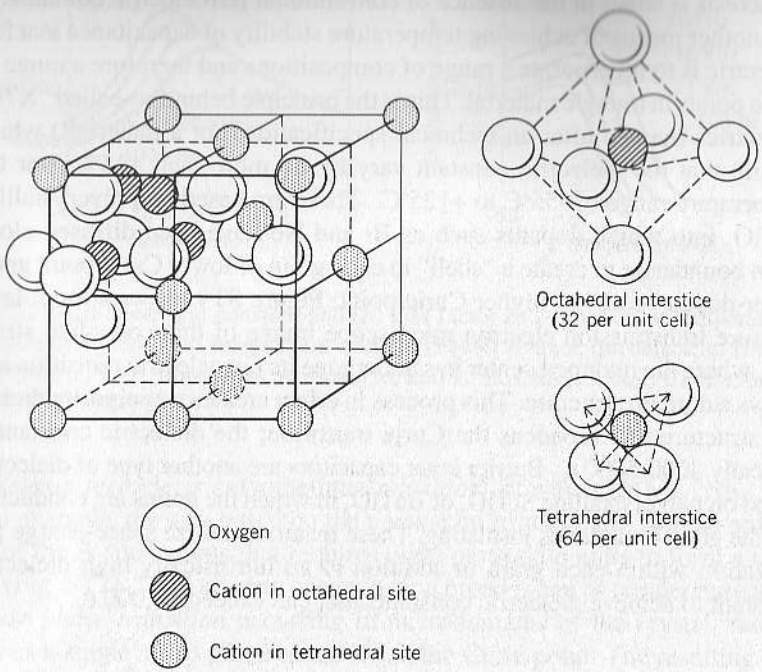

Fig. 1.30 Atomic layers parallel to the (001) plane in spinel.

as a solid solution between an ideal end member (normal or inverse) and a disordered spinel in which the site occupation is completely random. $MgAl_2O_4$ forms the highly ordered normal spinel structure only in its naturally occurring mineral form, in which slow crystallization over geologic times has allowed a high degree of ordering to take place. Synthetic $MgAl_2O_4$ that is grown at elevated temperatures and then cooled at laboratory rates is always disordered to some degree. Magnesium aluminate spinel is a highly refractory compound of some utility for structural and optically transmitting applications. The most commercially important spinel structure ceramics by far are soft magnetic ferrites, used in a broad range of applications such as inductors, transformer cores, and read/write heads for magnetic storage media.

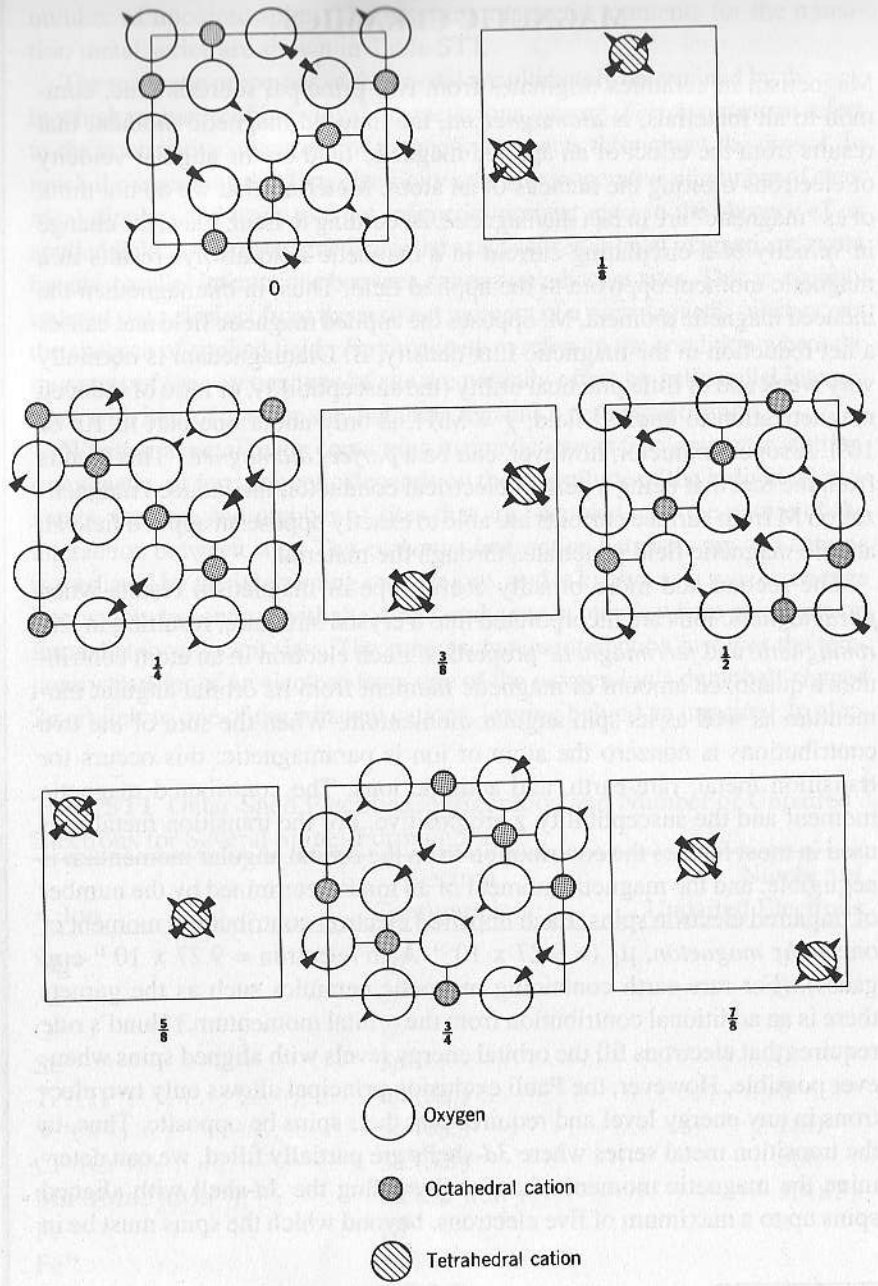

Fig. 1.31 Spinel structure. (From A. R. von Hippel, *Dielectrics and Waves*, John Wiley and Sons, New York, 1954.)

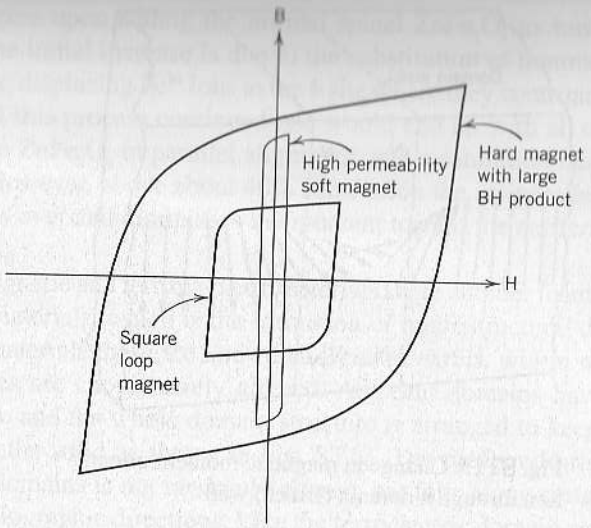

Fig. ST15 B-H loops representative of hard and soft magnetic materials.

initial permeability, μ_i. With increasing field, B increases until saturation is reached. If complete alignment of the material into a single domain is achievable then $B_s = \mu_0 H + \mu_0 M_s$, M_s being the saturation magnetization we discussed above. Normally microstructural factors and *domain wall pinning* by defects such as grain boundaries limit B_s to less than this ideal value. Upon removing the field, B decreases until at zero field a remnant magnetization B_r is left. If the field is reversed ($H<0$), there is a characteristic field necessary to achieve zero B, known as the *coercive field*, H_c.

The shape of the B-H loop characterizes whether a magnet is *hard* or *soft*. Figure ST15 compares several types of B-H loops useful for different magnetic applications. Permanent magnets are hard, and have both a high value of B_r, which is essentially the strength of the poled magnet after removing the field, and a high coercive field H_c, meaning that the magnet is difficult to demagnetize. The maximum of the product B · H, or *energy product* $(BH)_{max}$, is often used to characterize the strength of hard magnets. On the other hand, soft magnets such as the spinel ferrites are used in ac applications where a high saturation magnetization but low coercive field are desirable. These exhibit a narrow B-H loop. *Square loop* ferrites show sharply discontinuous changes in B at the coercive field and are useful in magnetic storage applications such as computer memory, and music and video tapes.

Perovskite / Rocksalt Derivatives: Cuprate Superconductors

In April of 1986, G. Bednorz and A. Mueller at IBM's Zurich laboratory reported signs of superconductivity in Ba-doped La_2CuO_4 at the then-unprecedented high temperature of 40 K. (Prior to this discovery, the highest temperature superconductor was in Nb_3Ge thin films, at 23 K.) Later that year, a group of researchers at the University of Tokyo led by K. Kitazawa reported a confirmation of this result, thereby sparking a world-wide search for new superconducting compounds that within two short years had resulted in the discovery of numerous additional cuprate compounds superconducting at temperatures as high as 125 K. R. J. Cava (pp. 3–8 in *Advances in Superconductivity V*, Y. Bando and H. Yamauchi, editors, Springer-Verlag, Tokyo, 1993) identified 34 structurally distinct cuprate superconductors which had been discovered by the end of 1992. Here, we will show how the family of cuprate superconductors may be considered derivatives of the perovskite and rocksalt structures, following a concise description by D. Smyth (pp. 1–10 in *Ceramic Superconductors II*, Research Update 1988, M. F. Yan, editor, The American Ceramic Society, 1988).

Several compounds of the simple perovskite structure type are superconducting. $SrTiO_3$ has a superconducting critical temperature, T_c, below which it is superconducting and above which it is a "normal" conductor, of less than 1 K. $BaPb_{1-x}Bi_xO_3$ (T_c~13K for $x = 0.25$) and $Ba_{1-x}K_xBiO_3$ (T_c~30 K for $x = 0.4$) are two

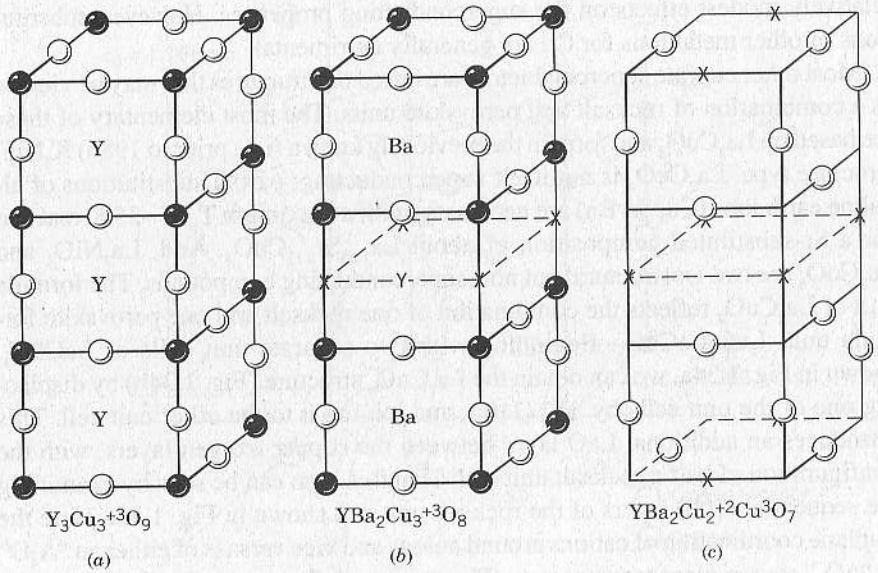

Fig. 1.32 Origin of the structure of $YBa_2Cu_3O_{7-x}$ as a triple-perovskite unit. (D. M. Smyth, pp. 1–10 in *Ceramic Superconductors II*, Research Update 1988, M. F. Yan, Ed. The American Ceramic Society, 1988.)

other examples. The high-temperature cuprate superconductor $YBa_2Cu_3O_{7-x}$, discovered by M.-K. Wu and C.-W. Chu in 1987, has a maximum T_c of about 93K, and is loosely based on a triple unit cell of "$YCuO_3$" perovskite, as shown in Fig. 1.32*a*. If two of the three Y^{3+} ions in this structure are substituted by Ba^{2+} ions, we have "$YBa_2Cu_3O_8$" and the structure shown in Fig. 1.32*b*. Charge neutrality has required the removal of one oxygen ion per formula unit, accommodated in this structure by oxygen vacancies around the central Y^{3+} ion. A distinctive characteristic of yttrium barium cuprate and most of the other superconducting cuprates is the existence of some copper in the Cu^{3+} valence state. In yttrium barium cuprate approximately one third of the total copper is trivalent, further reducing the oxygen content from our $Y_3Cu_3O_9$ reference state to $YBa_2Cu_2^{2+}Cu^{3+}O_7$. The additional oxygen vacancies are accommodated in the top and bottom-most copper planes (Fig. 1.32*c*). The resulting structure is shown in Fig. 1.33. Notice that there are two nonequivalent sites for copper, four-fold coordinated sites resulting in Cu-O "chains" oriented along [100] and five-fold coordinated sites forming layers of square pyramids joined at the corners. The oxygen stoichiometry (which varies proportionally with the copper valence state) is sensitive to temperature and oxygen pressure, and can vary between O_6 and O_7 depending on the annealing conditions. In optimized superconducting compositions the oxygen stoichiometry is about $O_{6.92}$, and is typically achieved by a low temperature (~500°C) annealing treatment in an oxidizing ambient. As the oxygen vacancies order along [100], the crystal symmetry correspondingly changes from tetragonal to orthorhombic. A number of isovalent substitutions can be made for Y and Ba in this structure with relatively modest effects on the superconducting properties. However, substitutions of other metal ions for Cu are generally detrimental.

Most other cuprate superconductors are based on structures that may be viewed as a combination of rocksalt and perovskite units. The most elementary of these are based on La_2CuO_4 and form in the previously known (i.e., prior to 1986) K_2NiF_4 structure type. La_2CuO_4 is not itself superconducting; partial substitutions of alkaline earth ions (Ca, Sr, Ba) are necessary, with a maximum T_c of ~35 K reached for a Sr-substituted composition of about $La_{1.85}Sr_{0.15}CuO_4$. And, La_2NiO_4 and La_2CoO_4 are two isostructural but non-superconducting compounds. The formula unit of La_2CuO_4 reflects the combination of one rocksalt and one perovskite formula unit: $LaO{\cdot}LaCuO_3$. Beginning with two separate unit cells of $LaCuO_3$, shown in Fig. 1.34a, we can obtain the La_2CuO_4 structure (Fig. 1.34b) by displacing one of the unit cells by $1/2\langle 110\rangle$, and joining it to the other unit cell. This introduces an additional LaO layer between the copper-oxygen layers, with the configuration of half a rocksalt unit cell. That this is so can be seen by examining the sequential (100) layers of the rocksalt unit cell shown in Fig. 1.35. Here the in-plane coordination of cations around anions and vice versa is of either an "A_4O" or "AO_4" square-planar arrangement. The structure follows an A_4O-AO_4-A_4O stacking sequence in the [001] direction. The same LaO_4-La_4O sequence can be seen between Cu-O layers in the La_2CuO_4 structure (Fig. 1.34*b*). Notice that the copper ion retains a six-fold coordination, whereas the La ions, being coordinated on one

side by a rocksalt-like structure (CN = 6) and on the other by perovskite (CN = 12), have a nine-fold coordination. La_2CuO_4 is tetragonal in symmetry, but alkaline earth substitutions cause a change to orthorhombic symmetry. The alkaline earth cations substitute for lanthanum in the structure. At lower concentrations (below $x \sim 0.2$ in $La_{2-x}Sr_xCuO_4$), the alkaline earth ions act as acceptors charge-compensated by electron holes (see Chapter 2 for discussion of electronic defects). The presence of an excess of holes is chemically equivalent to converting

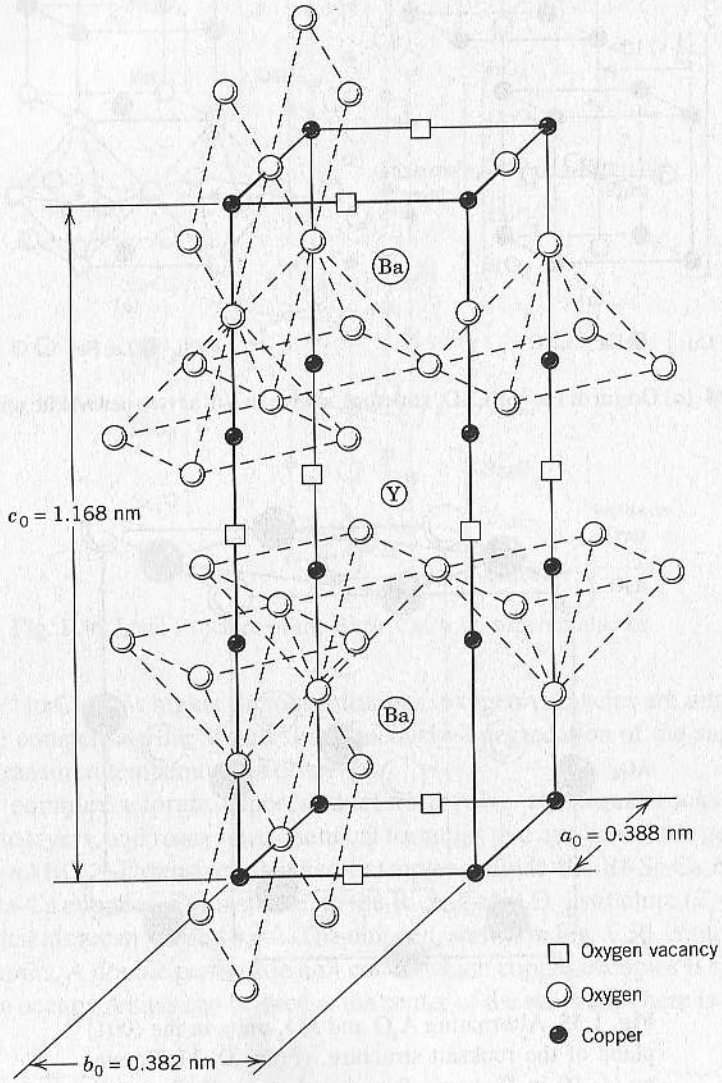

Fig. 1.33 $YBa_2Cu_3O_{7-x}$ structure showing four-coordinated copper in Cu-O chains and five-coordinated copper in Cu-O sheets.

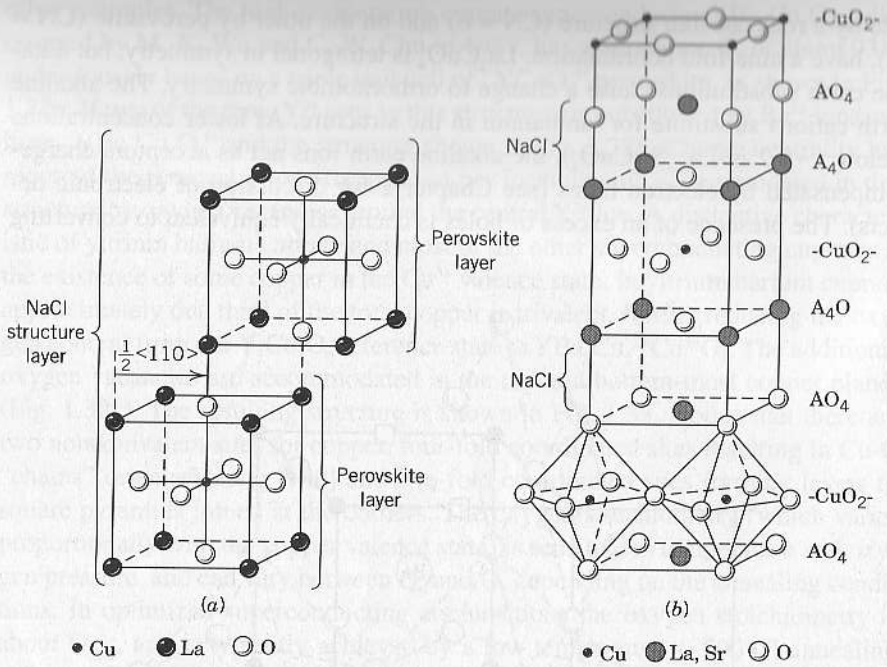

Fig. 1.34 (*a*) Origin of $La_{2-x}Sr_xCuO_4$ structure, shown in (*b*), as two perovskite unit cells.

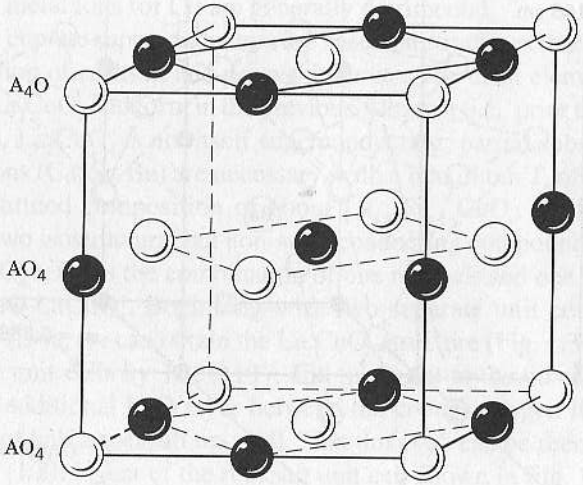

Fig. 1.35 Alternating A_4O and AO_4 units in the (001) plane of the rocksalt structure. (From D. M. Smyth, pp. 1–10 in *Ceramic Superconductors II*, Research Update 1988, M.F. Yan, Ed., The American Ceramic Society, 1988).

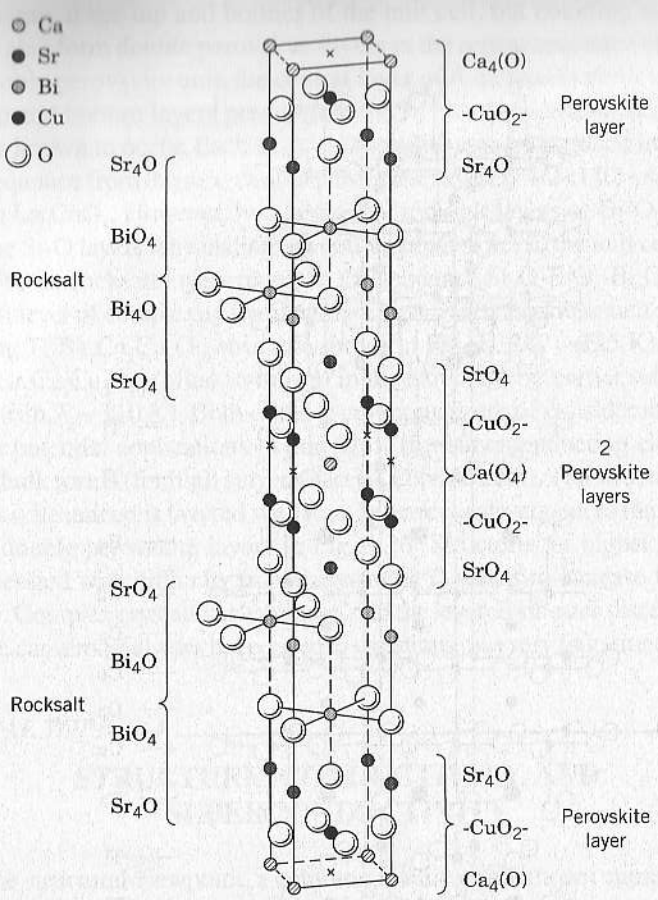

Fig. 1.36 Ideal structure of the $Bi_2Sr_2CaCu_2O_8$ superconductor.

some Cu^{2+} to Cu^{3+}. At higher Sr concentrations, oxygen vacancies are introduced to charge compensate the Sr and simultaneously a degradation of the superconducting transition temperature is observed.

More complex cuprate superconductors involve additional rocksalt and perovskite layers, and many have chemical formulas that can be written generally as $mAO \cdot nABO_3$.[4] Extensively studied examples include the Bi-Sr-Ca cuprates and Tl-Ba-Ca cuprates. For instance, in the $Bi_2Sr_2CaCu_2O_{8-\delta}$ structure ($T_c \sim 85$ K) the coefficients are $m = 3$ and $n = 2$. The unit cell, shown in Fig. 1.36, contains two formula units. A double perovskite unit cell in which copper occupies B sites and Sr and Ca occupy A sites can be seen at the center of the unit cell. There is a single

[4] Ruddlesden and Popper identified some time ago [*Acta Met.*, **11**, 54-55 (1958)] a similar class of structures in strontium titanate, based on the formula SrO-nSrTiO$_3$ (i.e., $m = 1$). These include $n = 1$ (Sr_2TiO_4), $n = 2$ ($Sr_3Ti_2O_7$) and $n = 3$ ($Sr_4Ti_3O_{10}$), all the way up to n = ∞ (the perovskite $SrTiO_3$).

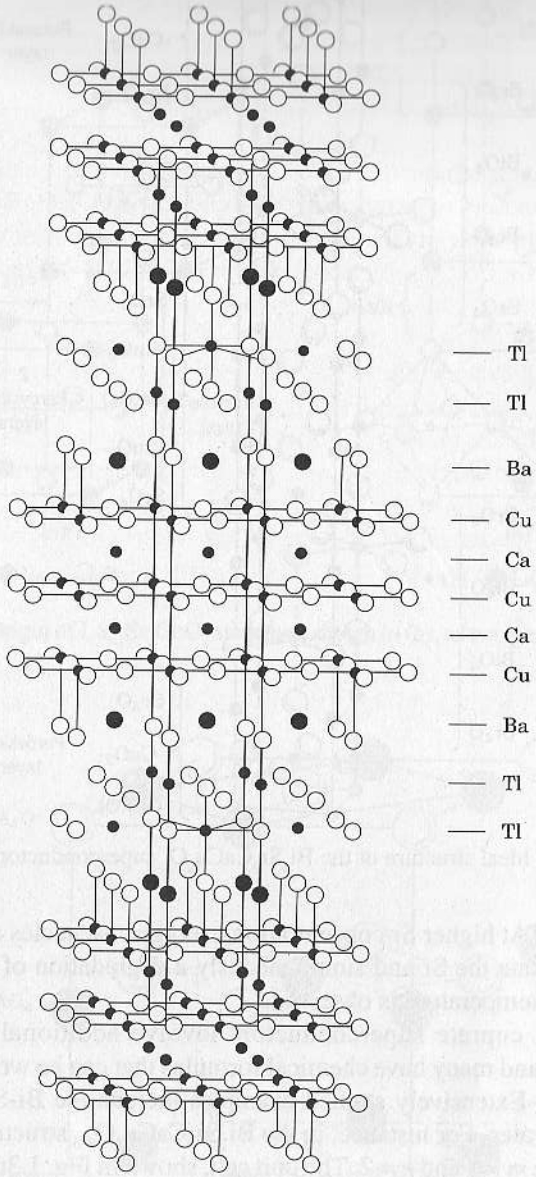

Fig. 1.37 Ideal structure of $Tl_2Ba_2Ca_2Cu_3O_{10}$ (From M. A. Subramanian, *Ceramic Transactions*, Vol. 13, K.M. Nair and E.A. Giess, Eds., The American Ceramic Society, 1990).

perovskite unit at the top and bottom of the unit cell, but counting adjacent unit cells these also form double perovskite layers in the repeat sequence of the lattice. In each double perovskite unit, the central layer of A cations is predominantly Ca and the top and bottom layers predominantly Sr, but considerable substitution of Sr for Ca is known to occur. Each double perovskite unit is displaced in the vertical stacking sequence from the next double perovskite layer by 1/2<110>, similar to the stacking in La_2CuO_4. However, two additional rocksalt layers of Bi-O also appear between the Sr-O layers terminating the double perovskite. In the unit cell depiction in Fig. 1. 36, the rocksalt layers repeat in the sequence Sr_4O-BiO_4-Bi_4O-SrO_4.

The next level of complexity involves $m = 3$, $n = 3$ compounds, such as the rather intimidating $Tl_2Ba_2Ca_2Cu_3O_{10}$ structure shown in Fig. 1.37 (T_c ~125 K) or its counterpart $Bi_2Sr_2Ca_2Cu_3O_{10}$ (often stabilized in this structure by partial substitution of Pb for Bi, with T_c ~ 110 K). Both of these compounds are of considerable technical interest for potential applications in thin films (for superconducting electronic devices) and bulk forms (for high current-carrying conductors). The structure contains triple perovskite unit cells layered with four-layer rocksalt sequences like those separating the double perovskite layers in Fig. 1.36. Structures of higher n have also been synthesized with difficulty in both systems; T_c seems to increase with n up to about $n = 5$. Complex crystals such as these, and the layered silicates discussed later in this chapter, can almost always be reduced to variations on a very few structural themes.

SPECIAL TOPIC 1.4

STRUCTURE, CONDUCTIVITY, AND SUPERCONDUCTIVITY

From the structural viewpoint, a common feature of all known cuprate superconductors is the existence of infinitely extending CuO_2 planes, separated by layers of alkaline earth or rare earth oxides. The bonding between copper and oxygen in these layers has a fair amount of covalent character, with electrons being shared between copper 3*d* and oxygen 2*p* orbitals. A second common characteristic is the existence of a significant fraction of copper in the trivalent state. This causes the electron energy band formed between copper and oxygen to be only partly filled; oxidation of copper from Cu^{2+} to Cu^{3+} leaves an electron hole in the conduction band and yields *p*-type conductivity. Partial band filling combined with weak localization of the valence electrons at atoms (low ionic character) results in a high electronic conductivity within the layer. The layered cuprates all show a strongly anisotropic electrical conductivity in the "normal" or nonsuperconducting state that is much higher in directions within the CuO_2 planes than it is normal to them. The resistivity generally shows a weak temperature dependence, sometimes decreasing with increasing temperature like a semiconductor but more often increasing with temperature like a metal (Fig. ST16 Also see Fig. 3.2). Thus the electronically active layers may be considered to be the CuO_2 planes. The intervening alka-

alumina substitution, including improved high-temperature oxidation resistance and a lower vapor pressure of the oxynitride spinel compared to silicon nitride. The latter makes it possible to densify β′ sialons without an overpressure of nitrogen to prevent decomposition, unlike pure silicon nitride. Other oxide substitutions besides Al_2O_3 are possible in β′ sialons, including Y_2O_3, MgO (as Mg_2SiO_4 substituted for Si_3N_4), and BeO ($BeAl_2O_4$ for Si_3N_4).

α′ sialons are based on a similar substitution into the α-Si_3N_4 structure, often with charge compensating cations such as Li^+, Ca^{2+}, and the rare-earths occupying the large interstitial sites. O′ sialons are solid solutions between Si_2N_2O and Al_2O_3; here the oxide alone has the correct stoichiometry for substitution. The polytypoid sialons based on AlN differ from these in that some of the Al^{3+} takes on an octahedral coordination. With increasing substitution of SiO_2 into the wurtzite AlN structure, the metal-anion ratio decreases and is accommodated by the substitution of Si^{4+} into tetrahedral positions and displacement of Al^{3+} into octahedral layers where it is coordinated by oxygen. These octahedral layers separate tetrahedral (Al, Si)N layers. With increasing substitution of SiO_2, new polytypoid phases are formed at integer ratios of metals to anions (e.g., 1:1 for AlN, 9:10 for 27R phase, 6:7 for 12H phase). Within each polytypoid, a range of solid solution exchanging Al^{3+} and Si^{4+} is possible as long as it is accommodated by a corresponding substitution between O^{2-} and N^{3-} for charge neutrality.

1.4 CRYSTALLINE SILICATES

A great many naturally occurring ores and minerals are silicates. According to the Si^{4+}/O^{2-} radius ratio, tetrahedral coordination is preferred. Pauling's electronegativities also indicate that the Si-O bond is 51% ionic and 49% covalent. The high degree of covalency favors tetrahedral coordination where in the $3s^23p^2$ outer electron shell of the Si atom is stabilized in a bonding configuration with four $3sp^3$ hybridized orbitals, as in the diamond cubic. Together this leads to a very strong preference for the formation of $(SiO_4)^{4-}$ tetrahedra in both crystalline and glassy silicates. In this configuration the bond strength of Si^{4+} is 4/4 = 1, and from Pauling's second rule an oxygen ion must be coordinated by two Si^{4+} in pure SiO_2. This mandates the corner sharing of $(SiO_4)^{4-}$ tetrahedra, a characteristic common to crystalline SiO_2, the silicate minerals, and silicate glasses alike. Corner sharing of oxide tetrahedra also prevents the close-packing of anion layers as in the FCC- and HCP- based oxides, and so crystalline silicates tend to have open structures.

Another feature of crystalline silicates is the ready substitution of other cations in place of the tetrahedrally coordinated Si^{4+}. The most important of these is Al^{3+}, which can adopt tetrahedral or octahedral coordinations. When substituted for Si^{4+}, a charge imbalance results that can be corrected by the substitution of an OH^- ion for O^{2-} (in the clay minerals) or by adding alkaline or alkaline earth cations in local interstitial sites (in glasses and crystalline silicates). Charge-compensating substitutions permit great flexibility in dissolving high concentrations of additives. Also, the $(SiO_4)^{4-}$ tetrahedron may no longer need to share all corners in order to satisfy Pauling's second rule. Silicate minerals can therefore be classified according to the connectivity between their silica tetrahedra.

Oxygen/Silicon Ratio

The O/Si ratio is a useful parameter for characterizing the degree of connectivity between silica tetrahedra in silicate compounds. This classification scheme is summarized in Table 1.4. It is also useful in characterizing the degree of connectivity in silicate glasses, which we discuss later.

Crystalline SiO_2 has an O/Si ratio of 2, which requires sharing of all four corners. It occurs in three basic crystalline polymorphs, cristobalite, tridymite and quartz, transformations between which are reconstructive (and sluggish). Each of these phases also has a *high* and *low* form related by a displacive transformation (tridymite also has a *middle* form) as shown in Table 1.5. The high form always has the higher symmetry. Cristobalite is the highest-temperature polymorph, shown in Fig. 1.39. It has some similarity to the zincblende structure (Fig. 1.16) but with tetrahedra substituted for atoms; note the sharing of all corners. Tridymite is monoclinic (high form) and is the intermediate-temperature structure. Quartz is hexagonal (low quartz is trigonal) and is the lowest-temperature form (Fig. 1.40).

With increasing O/Si ratio the number of shared corners decreases. The physical habit of the compound often refects its crystalline structure. For instance, layered silicate compounds such as talc, mica, and clay (O/Si = 2.5) contain $(Si_2O_5)_n$ sheets in which three corners of each tetrahedron are shared. These are described in greater detail below. Chain silicates, formed at O/Si ratios of 2.75 to 3, often have a fibrous habit. Pyroxenes, examples of which are enstatite ($MgSiO_3$) and jadeite, have single chains of $(SiO_3)_n^{2n-}$. Close examination of the fracture surface of jadeite (the semiprecious gemstone jade) reveals its fibrous nature. Amphiboles have double chains, $(Si_4O_{11})_n^{6n-}$. The most common examples are the fibrous asbestos minerals. In this O/Si range it is also possible to form structures with isolated rings of tetrahedra, such as beryl, $Be_3Al_2Si_6O_{18}$ (the basis of emerald), in which six-tetrahedron $Si_6O_{18}^{12-}$ rings form, and wollastonite, $CaSiO_3$, in which three-tetrahedron $Si_3O_9^{6-}$ rings form. Progressing then to O/Si = 3.5, one finds the pyrosilicates in which double tetrahedra of $Si_2O_7^{6-}$ can be found. Finally, orthosilicates, in which the O/Si ratio is 4, have completely isolated tetrahedra with intervening cations, as in the structures of olivine (forsterite, Mg_2SiO_4, and olivine, Fe_2SiO_4) and zircon ($ZrSiO_4$). Table 1.4 shows the systematic changes in structure between these classes of silicates.

Clay Minerals

Many of the common layered silicates such as clay, talc, and mica may be known to the reader. They are based on hydrated aluminosilicate structures in which $(Si_2O_5)_n$ sheets are joined to $AlO(OH)_2$ layers containing octahedrally coordinated

Table 1.4 Effect of Oxygen-Silicon Ratio on Structure in Silicates

O/Si Ratio	Silicon-Oxygen groups	Silicate structure	Examples
2		SiO_2 (completely interconnected tetrahedra)	Quartz, tridymite, cristobalite
2.5	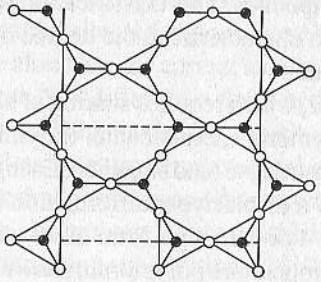	Si_4O_{10} (sheets)	Talc, mica, kaolinite, montmorillonite clays, vermiculite
2.75	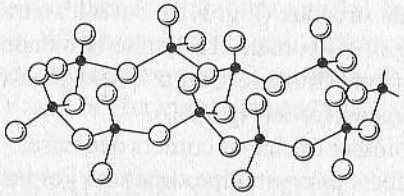	Si_4O_{11} (chains)	Amphiboles (asbestos minerals)
3	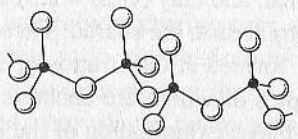	SiO_3 (chains or rings)	Pyroxenes (chains), beryl (rings)
	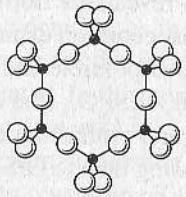		
3.5	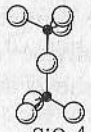 SiO_4^{4-}	Si_2O_7 (tetrahedra sharing one oxygen ion)	Pyrosilicates
4	 $Si_2O_7^{6-}$	SiO_4 (isolated tetrahedra)	Orthosilicates (forsterite, olivine, zircon)

Table 1.5 Polymorphic Forms of Silica

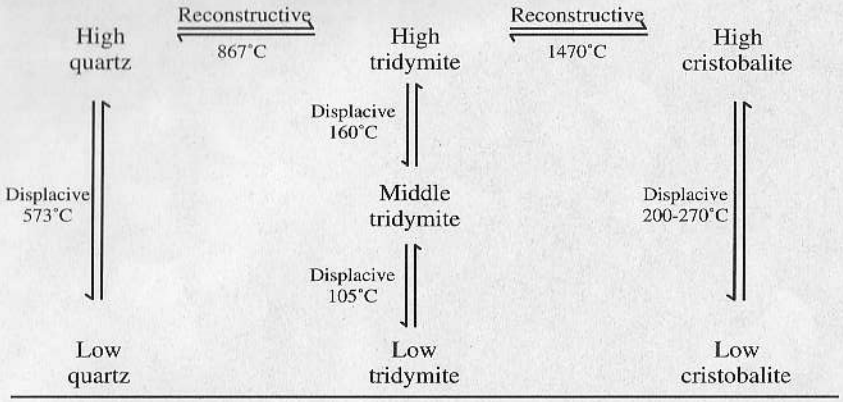

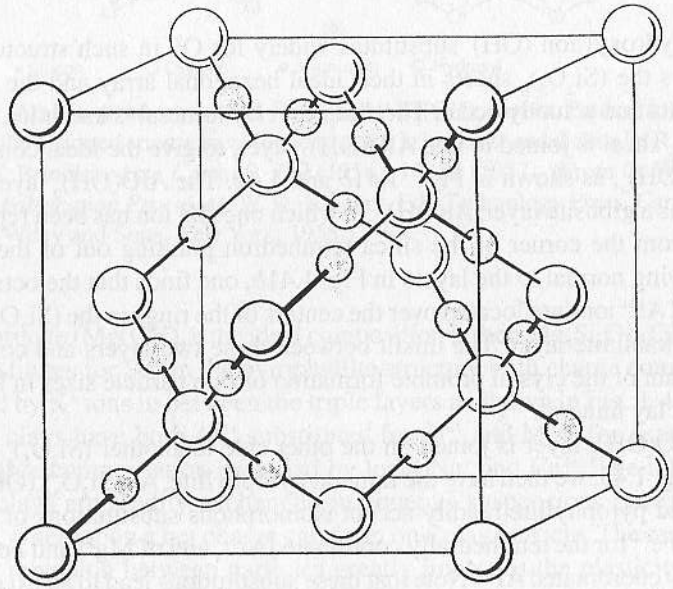

Fig. 1.39 Structure of high cristobalite.

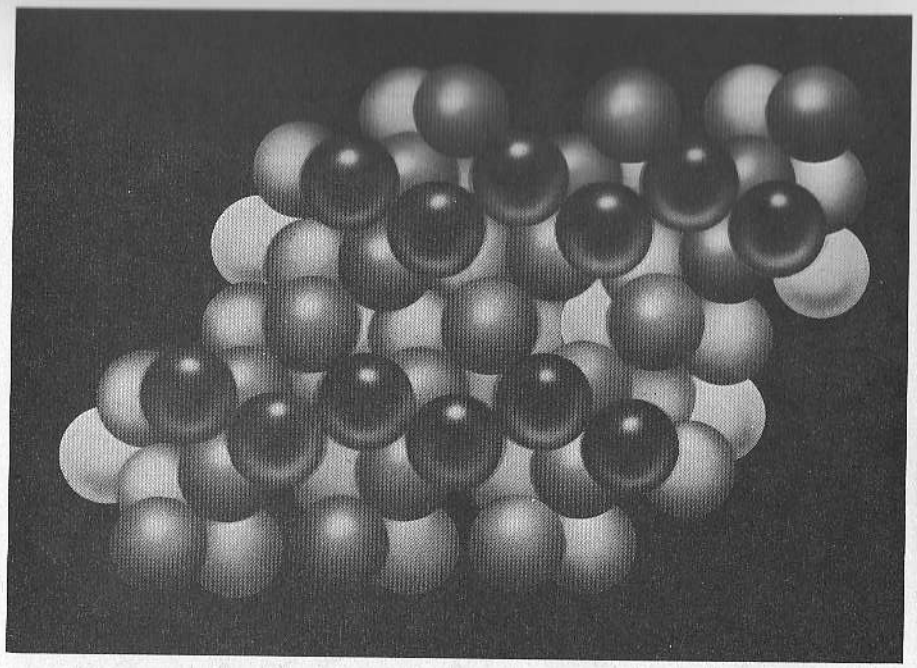

Fig. 1.40 Structure of high quartz, looking down on the basal plane.

Al^{3+}. The hydroxyl ion $(OH)^-$ substitutes widely for O^{2-} in such structures. Fig. 1.41*a* shows the $(Si_2O_5)_n$ sheets in their ideal hexagonal array and the distorted arrangements that actually occur. The simplest clay mineral is kaolinite, in which one $(Si_2O_5)_n$ sheet is joined to one $AlO(OH)_2$ layer, to give the ideal composition $Al_2(Si_2O_5)(OH)_4$, as shown in Figs. 1.41*b* and 1.42. The $AlO(OH)_2$ layer may be thought of as a gibbsite layer, $Al(OH)_3$, in which one OH ion has been replaced by an O ion from the corner of the silica tetrahedron pointing out of the $(Si_2O_5)_n$ sheet. Viewing normal to the layers in Fig. 1.41*b*, one finds that the octahedrally coordinated Al^{3+} ions are located over the centers of the rings in the $(Si_2O_5)_n$ sheets of the next kaolinite layer. The misfit between these two layers and consequent bending strain of the crystal promote formation of fine particle sizes in kaolinite, a common clay mineral.

If the $AlO(OH)_2$ layer is joined on the other side to another $(Si_2O_5)_n$ sheet, as shown in Fig. 1.43, we then have the mineral pyrophyllite, $Al_2(Si_2O_5)_2(OH)_2$. Both kaolinite and pyrophyllite readily accept isomorphous substitutions of Al^{3+} and sometimes Fe^{3+} for the tetrahedrally coordinated Si^{4+}, and of Mg^{2+} and Fe^{2+} for the octahedrally coordinated Al^{3+}. Note that these substitutions lead to an excess negative charge on the layers, which is typically compensated by interstitial cations between the layers. The type of substitution and the way in which the charge imbalance is accommodated distinguish the specific clay minerals. For instance, talc is similar to pyrophyllite except that the gibbsite $(Al(OH)_3)$ central layer is

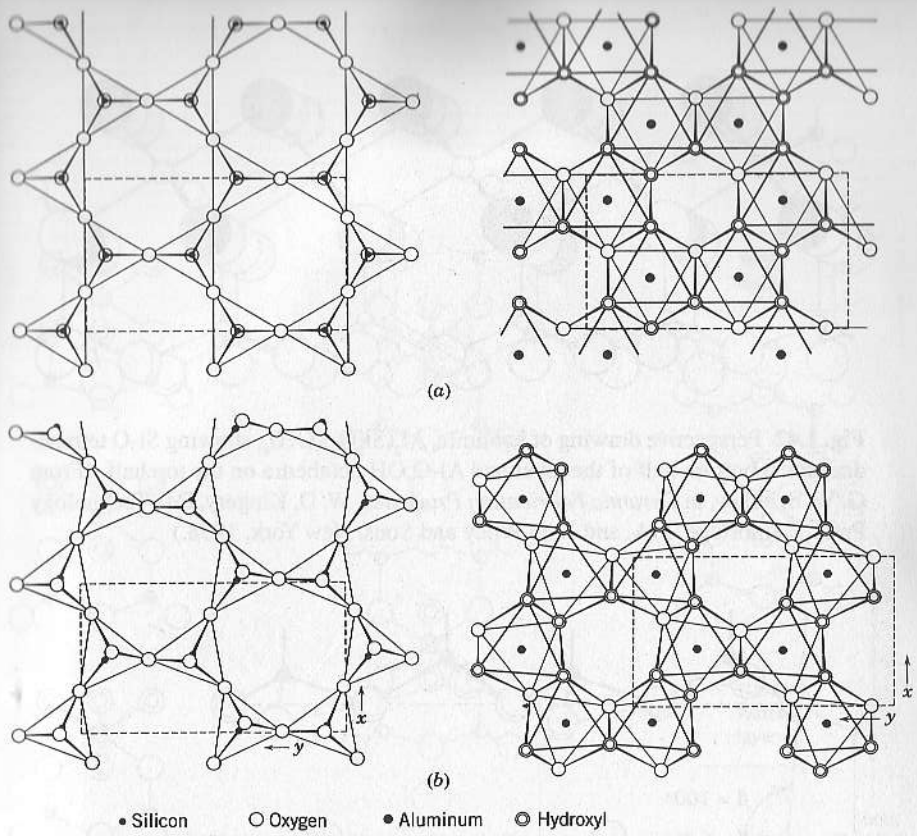

Fig. 1.41 Atomic arrangements of Si_2O_5 and $AlO(OH)_2$ layers. Pattern (*a*) is idealized, and (*b*) is the distorted arrangement found to occur in kaolinite and dickite by R. E. Newnham and G. W. Brindley, *Acta Cryst.*, 9, 759 (1956); 10, 89 (1957). (From G. W. Brindley, in *Ceramic Fabrication Processes*, W. D. Kingery, Ed., Technology Press, Cambridge, MA, and John Wiley and Sons, New York, 1958.)

instead brucite $(Mg(OH)_2)$; the ideal composition is then $Mg_3Si_4O_{10}(OH)_2$. In mica, Al^{3+} substitutes for Si^{4+} in the pyrophyllite structure with charge compensation is provided by K^+ ions in between the triple layers as shown in Fig. 1.44. Montmorillonite clays have both Al^{3+} substituted for Si^{4+} and Mg^{2+} for octahedral Al^{3+}, with charge compensation provided by local Na^+ and Ca^{2+}. The interlayer cations in clays are readily exchanged in aqueous suspensions (termed base exchange), whereupon a net charge can form on a clay particle. The resulting electrostatic repulsion between particles greatly improves the plasticity and forming characteristics of a clay-water suspension, as is well-known by potters. (This effect is the historical origin of the electrostatic stabilization of ceramic powder slurries, now understood and practiced in ceramics processing at a highly sophisticated level.)

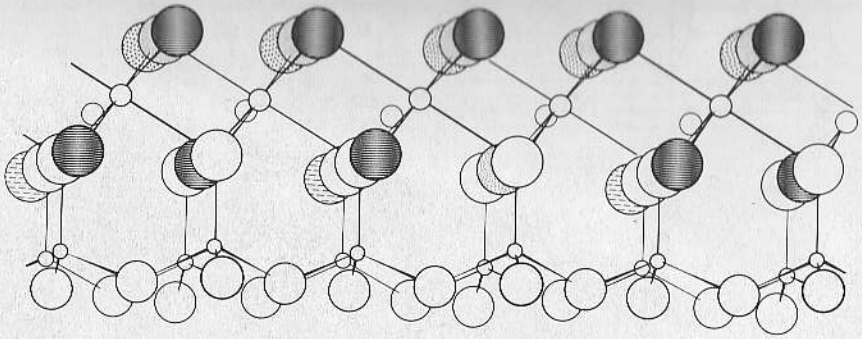

Fig. 1.42 Perspective drawing of kaolinite, $Al_2(Si_2O_5)(OH)_4$, showing Si-O tetrahedra on the bottom half of the layer and Al-O,OH octahedra on the top half. (From G. W. Brindley, in *Ceramic Fabrication Processes*, W. D. Kingery, Ed., Technology Press, Cambridge, MA, and John Wiley and Sons, New York, 1958.)

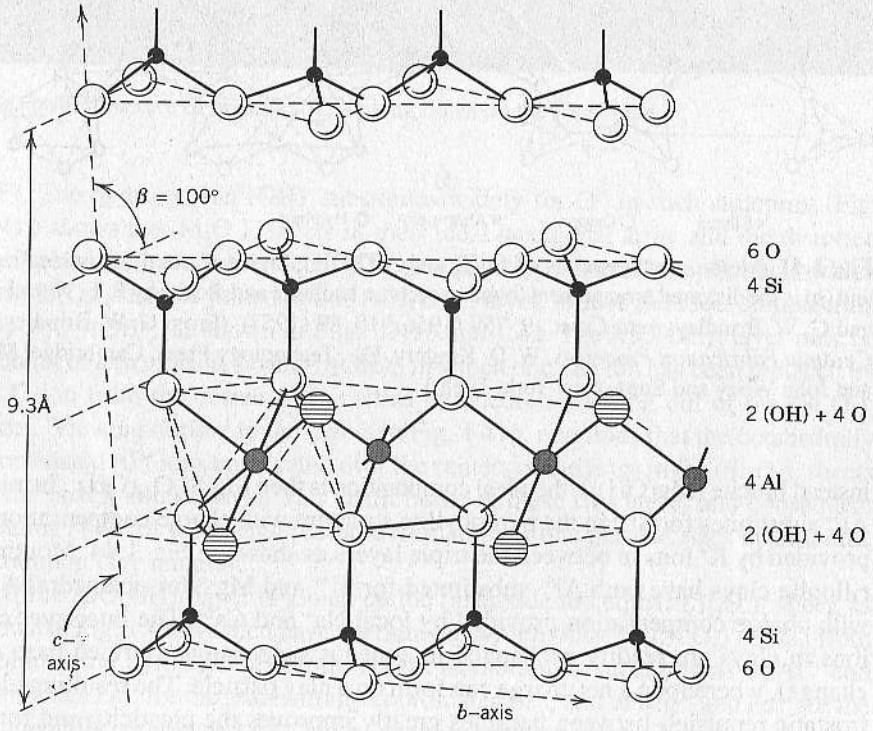

Fig. 1.43 Structure of pyrophyllite, $Al_4(Si_4O_{10})_2(OH)_4$, showing joining of two layers of tetrahedrally coordinated Si-O to a central octahedral Al-O,OH layer.

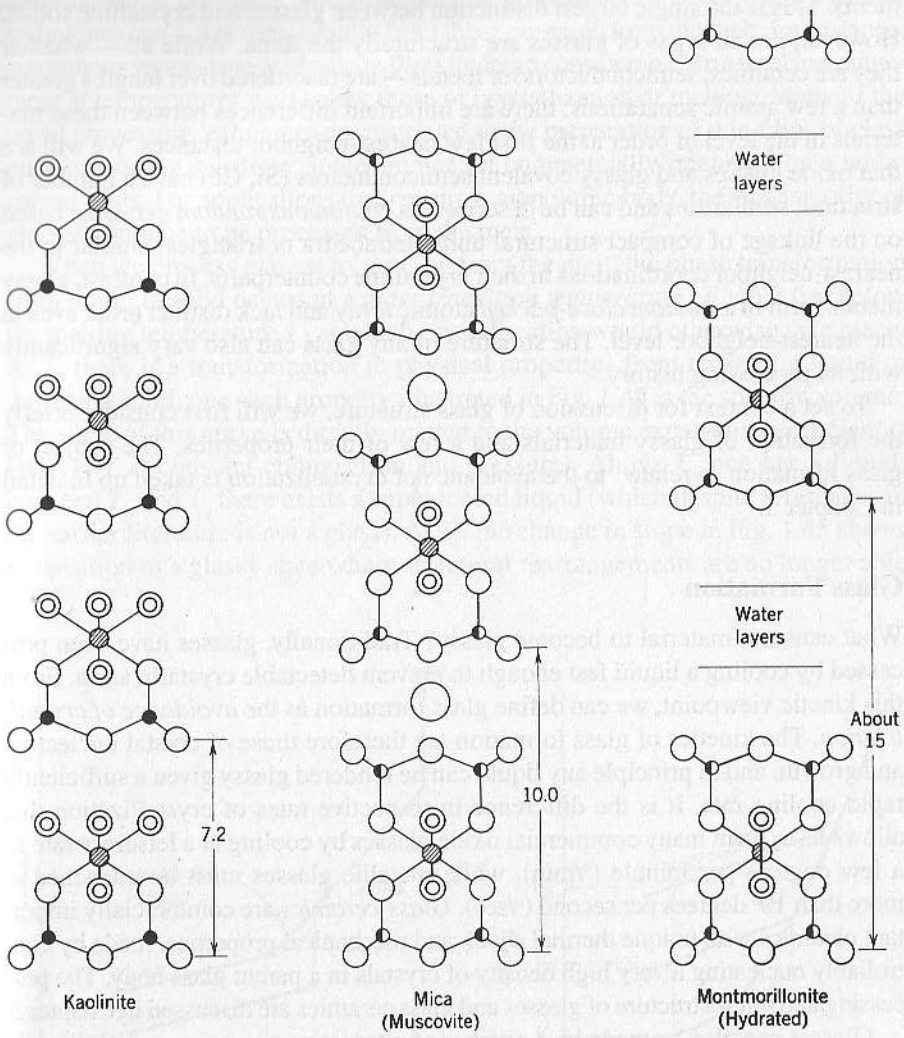

Fig. 1.44 Layer structure of clay and similar materials. (From G. W. Brindley, in *Ceramic Fabrication Processes*, W. D. Kingery, Ed., Technology Press, Cambridge, MA, and John Wiley and Sons, New York, 1958.)